Relative sea-level change in Greenland during the last 700 years and ice sheet response to the Little Ice Age

Antony J. Long*[1], Sarah A. Woodroffe[1], Glenn A. Milne[2], Charlotte L. Bryant[3], Matthew J.R. Simpson[4] and Leanne M. Wake[4]

[1]Department of Geography, Durham University, Science Site, South Road, Durham DH1 3LE, UK, a.j.long@durham.ac.uk, s.a.woodroffe@durham.ac.uk
[2]Department of Earth Sciences, University of Ottawa, Marrion Hall, Ottawa, K1N 6N5, Canada, gamilne@uottawa.ca
[3]NERC Radiocarbon Laboratory, Scottish Enterprise Technology Park, Rankine Avenue, East Kilbride, Glasgow, G75 0QF, UK, c.bryant@nercrcl.gla.ac.uk
[4]Department of Earth Sciences, Durham University, Science Site, South Road, Durham, DH1 3LE UK, matthew.simpson@statkart.no, lwake@ucalgary.ca

*Corresponding author
Phone: +44 191 334 1913
Fax: +44 191 334 1918
Email: A.J.Long@Durham.ac.uk

Abstract

This paper presents new evidence regarding relative sea-level (RSL) changes and vertical land motions at three sites in Greenland since 1300 A.D., a time interval that spans the later part of the Medieval Climate Anomaly (MCA) and the Little Ice Age (LIA). We observe RSL rise at two sites in central west Greenland from c. -0.80 ± 0.20 m at c. 1300 A.D. to c. -0.20 m ± 0.25 m at c. 1600 A.D., after which RSL slowed and then stabilised. At a third site in south Greenland, we observe RSL rise from c. -1.40 ± 0.20 m at c. 1400 A.D. until c. 1750 A.D., after which RSL slowed and was stable during at least the latter part of the 20th century. The c. 1600 A.D. RSL slow-down seen at the two former sites is surprising because it occurs during the LIA when one might expect the ice sheet to be gaining mass and causing RSL to rise. We interpret this RSL slowdown to indicate a period of enhanced regional mass loss from central west Greenland since c. 1600 A.D and propose two hypotheses for this loss: first, a reduction in precipitation during cold and dry conditions and second, higher air temperatures and increased peripheral surface melt of the ice sheet from this date onwards. The latter hypothesis is compatible with a well-established temperature seesaw between western Greenland and northern Europe and, potentially, a previously

identified shift from a positive to generally more negative NAO conditions around 1400 to 1600 A.D. Our study shows how RSL data from Greenland can provide constraints on the timing of ice sheet fluctuations in the last millennium and challenges the notion that during cold periods in northern Europe the ice sheet in west Greenland gained mass.

Keywords
Neoglacial, relative sea level, crustal motions, Greenland Ice Sheet, Little Ice Age, North Atlantic Oscillation

1. Introduction

Vertical land motions measured at sites around the margins of an ice sheet are strongly influenced by changes in adjacent ice load over annual to millennial timescales. Ongoing and recent GPS campaigns in Greenland record elastic rebound >10 mm/a at sites adjacent to the margins of several major outlet glaciers that are losing significant ice mass (Dietrich et al., 2007; 2005; Khan et al., 2010; Khan et al., 2007). Longer-term and more gradual viscous land motions are important at sites distant from these areas.

GPS records extend back only a decade or so and therefore alternative data sets must be used to accurately capture longer-term trends that recent elastic changes are superimposed upon. Relative sea-level (RSL) observations provide one such source of data. Previous work in Greenland addresses large scale (130 m +) changes in RSL since the last glacial maximum (Funder and Hansen, 1996; Long et al., 2008; Long et al., 1999; Sparrenbom et al., 2006b; Weidick, 1972), but there are no studies of regional trends in RSL during the last millennium. These are needed if we are to understand how the ice sheet responded to periods of past warmer or cooler than present conditions, notably during the Medieval Climate Anomaly (MCA) and the Little Ice Age (LIA).

We present RSL histories for three sites in west Greenland (Aasiaat (Disko Bugt), Sisimiut and Nanortalik, Figure 1) developed from salt marsh deposits that date from c. 1300 A.D. to the present. We identify a marked slow-down in RSL rise at Aasiaat and Sisimiut that dates to c. 1600 A.D., and a less well defined deceleration at Nanortalik sometime in the last 200 years. If these trends reflect changes in the GIS, they imply a loss of ice mass in central west Greenland during the last 400 years that began during the LIA, whilst a similar change in south Greenland dates from towards the end of the LIA. This work is important since it identifies, for the first time, evidence for regional trends in RSL and vertical land motions in

west and south Greenland that show an unexpected relationship between changes in ice sheet load and palaeoclimate.

1.1 The Little Ice Age in Greenland

The 'Little Ice Age' is a term widely used in climate and glaciological literature. Some authors use it in a climatic sense, referring to a period of variable but generally cooler than present conditions that ended in the late 19th century, prior to the warming of the 20th century (Lamb, 1977). Others associate the term with periods of glacier or ice sheet advance (Grove, 1988). This inconsistency has led some (e.g. Ogilvie and Jonsson, 2001) to recommend that the term not be used, instead preferring to simply recognise that the period between 1250 A.D. and 1900 A.D. was, on average, slightly cooler than during the 20th century.

There is geomorphic evidence that in many areas the GIS has retreated during the 20th century. Indeed, in parts of east and southwest Greenland, the prominent recent moraines of the "historic" period (Christiansen, 1998; Weidick, 1972) record the most extensive ice margin position during the entire Holocene (e.g. Hall et al., 2007; Kelly and Lowell, 2009; Weidick and Bennike, 2007). However, the details of LIA ice margin changes in Greenland are poorly understood and in many cases dates provide only evidence of when retreat from their maximum extent began, not when ice build-up actually occurred.

Evidence from some sites in west Greenland suggests that the maximum "historic" position was attained by the start of the 18th century (Weidick, 1972). However, several authors present evidence that local ice margins had advanced several centuries prior to this time. Thus, Bennike and Sparrenbom (2007) establish a minimum age for the formation of a prominent valley moraine in south Greenland that is several kilometres in front of the present ice sheet margin to c. 800 A.D. In the same region, Kaplan et al. (2002) infer a glacier advance into a lake catchment from c. 1000 A.D., representing the most advanced ice margin position during the late Holocene. Further north at Kangerlussuaq (Figure 1), Forman et al. (2007) date neoglacial moraines a few tens of meters in front of LIA moraines to c. 1200 a B.P. (c. 750 A.D.) suggesting that here as well the ice sheet was more extensive before the start of the LIA. In Disko Bugt (Figure 1) there is cartographic and archival evidence that the Jakobshavn ice stream terminus was advancing before 1850 A.D. (Weidick and Bennike 2007). Recent sedimentological data from threshold lakes indicate that the initial stages of this advance may have been as early as 1600 A.D. to the north of

Jakobshavn (Briner et al., 2010), and that the southern margin of the ice stream was close to its present position by c. 2000 a BP.

Greenland ice cores reveal complex spatial and temporal variations during the last 800 years. According to down-core temperature records from the GRIP and DYE3 ice cores, temperatures fell after c. 900 A.D. to reach a minimum at c. 1500 A.D. This was followed by a relatively warm interval and a second minimum at c. 1850 A.D. (Dahl-Jensen et al., 1998; Johnsen et al., 2001). Ice core accumulation data suggest little evidence for persistent changes during the period after 1200 A.D. (Andresen et al., 2004) although Deuterium and Na^{++} records all point towards a significant change in moisture source after c. 1400 A.D. that may record a strengthening of meridional circulation (Dawson et al., 2007; Hoffmann et al., 2001; Kreutz et al., 1997; Mayewski et al., 1993).

1.2 Controls on Greenland relative sea-level change during the late Holocene

It is useful to briefly review observational evidence for RSL changes during the late Holocene near our data sites and the processes thought to be responsible for these. This information provides the context required to interpret the salt marsh reconstructions presented below.

RSL reconstructions from isolation basin deposits indicate a change from sea-level fall to rise at our three sites. At Aasiaat and Sisimiut, these data indicate that a minimum in RSL, a few metres below present sea level, occurred between 3 to 1 cal ka BP (Long et al., 2003; Long et al., 2009). At Nanortalik, the data indicate an earlier and deeper RSL minimum (-8 m between 8 and 6 cal ka BP). A handful of modelling studies (Tarasov and Peltier, 2002; Fleming and Lambeck, 2004; Simpson et al., 2009) have interpreted this change as being due to the transition from uplift dominated (driven by GIS deglaciation) to subsidence dominated RSL change. These studies suggest that the subsidence is driven by two processes: a significant re-growth of the south west sector of the ice margin during the neoglacial (c. 4 to 2 cal ka BP) and peripheral bulge subsidence associated, largely, with the deglaciation of North American ice. The relative contribution of these processes is not well agreed upon and likely varies with location. We note that changes in global land ice volume is constrained to be small (order decimetre per ka) since c. 2 cal ka BP (e.g. Lambeck et al., 2004) and so the observed late Holocene RSL rise is predominantly due to vertical land motion.

The steady RSL rise due to land subsidence is the baseline signal that contemporary changes will be superimposed upon. As introduced above, the primary departure from this trend evident in the salt marsh deposits is the change to zero rate of rise (to with observational uncertainty) at around 1600 A.D. at Aasiaat and Sisimiut and between 1750-1950 A.D. at Nanortalik. We make a qualitative interpretation of this departure in Section 3.2.

1.3 Salt marshes and RSL reconstruction in Greenland

Small salt marshes exist in protected coastal settings along much of the west coast of Greenland. Like their mid-latitude counterparts, they can act like long-term natural tide gauges and record in their sediments evidence for RSL change. The precision of salt marsh RSL reconstructions (typically ± 0.20 m (Woodroffe and Long, 2009, 2010)) is much better than for drowned isolation basins (± 0.50 m or more) (Long et al., 2006; Sparrenbom et al., 2006b), archaeological data or raised beaches.

The only previous salt marsh study in west Greenland, from a site close to Sisimiut (Figure 1), records rapid RSL rise from -0.60 ± 0.20 m at 1350 A.D. to reach -0.10 ± 0.20 m at c. 1600 A.D. (Long et al., 2010). After this time, RSL stabilised and remained close to present (-0.10 ± 0.25 m) until present. It is not clear whether the trends observed at Sisimiut are representative of elsewhere in west Greenland. However, differences between Holocene RSL data, GIA model predictions and GPS data all suggest that different parts of the ice sheet are likely to record distinct RSL signatures during the last millennium (Simpson et al., 2009). We now present two new salt marsh RSL records from sites to the south and north of Sisimiut to reconstruct regional patterns in RSL since 1300 A.D.

2. Material and methods

2.1 Field sites

The location of our three field sites are shown in Figure 1 and tidal and meteorological data for each are listed in Table 1. Detailed descriptions of each site are included in supplementary information. Sea ice affects all three sites and there is geomorphic and sedimentary evidence for disturbance of the tidal flat and low marsh environments, including ripped up blocks of salt marsh that have been transported landwards, as well as coarse debris deposited on the marsh surface by ice blocks. The contemporary vegetation at each marsh typically comprises upland communities of *Empetrum nigrum* heath or freshwater marsh that are replaced by *Carex*-rich high marsh (Figure 2). The high marsh extends

downwards to close to the level of Mean High Water of Spring Tides (MHWST) where low marsh dominated by *Puccinellia phyryganodes* occurs and grades downwards into tidal flat.

2.2 Methods

We reconstruct RSL by studying contemporary and fossil diatom distributions (microscopic single-celled plants with particular salinity tolerances), organic content and grain size data, together with the radiocarbon dating of terrestrial plant macrofossils from salt marshes at Nanortalik (south Greenland) and Aasiaat (Disko Bugt, west Greenland). We use these data to reconstruct how the palaeomarsh surface elevation and hence RSL changes over time.

We surveyed all samples to mean tide level (MTL), established at each site by deploying a sea bed pressure transducer during fieldwork, and then related our observations to tidal data for the nearest coastal town (Royal Danish Administration of Navigation and Hydrography, personal communication). We collected contemporary samples for diatoms, percentage loss on ignition (%LOI) and particle size analysis (PSA) at regular vertical intervals from several transects across modern salt marshes and tidal flats at each site (see Long et al. (2010) for details).

We studied the stratigraphy of the salt marshes using shallow trenches, targeting sites where deposits overlie bedrock to minimise the effects of frost heave and sediment compaction. The typical stratigraphy at each site comprises a basal freshwater peat that overlies bedrock and is conformably overlain by salt marsh sediment that extends to present surface (Figure 2). The total sediment thicknesses are generally less than 0.20 m. This stratigraphy records a drowning of former freshwater environments and a landwards and vertical migration of salt marsh conditions. Erosion of sediments from the tidal flat limits the height and age range of the sediment sequences available for analysis to the last 1-1.5 m and c. 700 yrs of deposition.

Sediment blocks for laboratory analysis were cut from free faces, wrapped in cling film and returned to Durham University where they were stored at 4°C. We extracted terrestrial plant macrofossils from 1 cm-thick sediment slices that we dated at the NERC Radiocarbon Laboratory and SUERC AMS Laboratory in East Kilbride, Scotland. Our approach has been to obtain one or two radiocarbon dates from each sediment block, normally from the transition between the freshwater peat and the overlying salt marsh because this provides the most precise palaeo-sea level indicator and also the most abundant material for dating. Our sea level record from each site therefore comprises data from multiple sediment

sections collected from different elevations in the intertidal zone. Radiocarbon dates are calibrated using the Oxcal calibration program (v.4 Bronk Ramsey, 1995; 2001) and are cited in year A.D. with a two sigma age range (unless stated otherwise) (Table 2 and supplementary information).

Diatoms are single celled, microscopic plants whose distribution on salt marshes are strongly controlled by salinity and hence flooding frequency and their elevation in the tidal frame. We have studied the contemporary distribution of diatoms across our target salt marshes to establish the elevation preference of different taxa. We quantify this information using a transfer function (TF) that models the vertical relationship between modern surface diatom assemblages and their elevation (m MTL). When diatoms die they become trapped and preserved in the accumulating salt marsh sediment. We extract these fossil diatoms from salt marsh sediment profiles deposited in the last 700 years and use the contemporary TF to reconstruct quantitative records of palaeomarsh surface elevation and hence RSL. Woodroffe and Long (2010) compare the diatom assemblages from the Aasiaat and Sisimiut marshes and observe that certain diatom species occupy different elevation ranges at each site, meaning that local training sets are required for TFs at each study site. Long et al. (2010) argue that TFs developed from these Greenland marshes may over- or under-estimate palaeo-marsh surface elevations (and hence sea-level) and instead use a visual assessment (VA) method that places weight on certain key taxa that change abundance at clearly defined elevations. We use both methods here.

The total vertical error term for each sea-level data point is calculated as the root squared error arising from estimates of survey error, tidal range uncertainty, and the sample specific reconstruction uncertainty associated with the TF and VA methods. The latter are calculated using the Root Mean Square Error of Predicition (RMSEP) and the range of the selected species respectively (Table 2 and S2). Frost heave may introduce some vertical scatter to our data but we cannot quantify this term at present because a lack of any direct observations of this process.

2.3 Results

We plot RSL reconstructions from our three study sites in Figure 3. All three datasets record an overall rise in sea level of at least 1 m during the last 800 years, although the trends differ. Data from our two central west coast sites are broadly similar and show RSL rising from c. 1300 A.D. to reach close to present (-0.20 ± 0.25 m) at c. 1600 A.D. In contrast at

Nanortalik RSL continues to rise until c. 1750 A.D., with a subsequent slow-down and approximate RSL stability in at least the latter part of the 20th century.

There is a notable age and altitude scatter to the data, despite our best efforts to maximise the precision of our reconstructions. For example, the visual assessment (VA) reconstructions have a vertical scatter of up to 0.50 m at Aasiaat and Sisimiut between c.1300 and 1600 A.D. Some of this reflects the natural variability in the diatom assemblages observed in fossil and contemporary environments, but some also reflects dating uncertainties. Sedimentation rates are slow on these Greenlandic marshes, typically several times slower than the prevailing rate of RSL change. As a result, a 1-cm thick slice of sediment used to extract diatoms and plant macrofossils for dating may include material that has accumulated over several decades. The radiocarbon calibration curve itself also introduces an unavoidable structure to the data by clustering ages towards three discrete time windows (c. 1300-1400 A.D., 1500-1600 A.D. and 1750-1800 A.D.) (Figure 3). During some of these intervals RSL was changing, as indicated by the diatom floras, but the calibration curve ascribes a similar age to the dated samples. We do not, therefore, interpret this clustering as evidence for discrete "jumps" in RSL or as evidence for uncertainties in the vertical reconstruction of the diatom models used.

The VA reconstructions generally plot lower than comparable transfer function (TF) estimates, have smaller height uncertainties and reduced sample scatter (Figure 3). The reasons for this include the sensitivity of the TF to diatom species optima and tolerances that occur at the upper and lower end of the contemporary training sets, whereas the VA method relies on certain indicator species that occur at narrowly defined levels in the upper part of the intertidal zone (Long et al., 2010). The larger vertical scatter in the TF reconstructions is also due to the impact that occasional peaks in certain diatom taxa have on elevation reconstructions, something that the VA method overcomes by considering other stratigraphic evidence (such as organic content and vertical diatom succession).

Several of the TF reconstructions suggest RSL rose up to 0.8 m (most are up to 0.4 m) above present after c. 1500 A.D. and then fell to present (Figure 3). We are suspicious of these reconstructions because we see no evidence for such a rise and then fall in our sediments, either in their lithology or their biostratigraphy. A 0.4 m rise and then fall in RSL would be sufficient to transform the spatial and vertical distribution of different salt marsh habitats and diatom floras. Moreover, as noted above (see also Woodroffe and Long (2009)), the species optima for several diatom taxa are over-predicted and this increases the RSL reconstruction.

There are no radiocarbon dated sea level index points dates after 1800 A.D. from Sisimiut and Aasiaat or between 1750 A.D. and c. 1950 A.D. from Nanortalik. The trend in RSL at these sites during these time periods is uncertain; it is possible that RSL rose above present and then fell or slowed and remained broadly stable to present (Figure 3). We use the diatom data from the multiple salt marsh sediment profiles to discriminate between these models. In Figure 4 we plot trends in RSL reconstructed from each of our salt marsh diatom profiles (full data are in supplementary information). We establish an age model for each profile by assuming constant sedimentation since the youngest radiocarbon date available from each. We divide the data into profiles that comprise low and high marsh samples, arguing that the latter are more reliable because of reduced risk of physical disturbance by sea ice and wave erosion. We use the TF reconstructions for Aasiaat and Sisimiut but, because of the differences between the contemporary and fossil data from Nanortalik, use the VA reconstructions from this site.

All Sisimiut profiles reconstruct MTL within a range of +0.4 m and -0.4 m MTL since c. 1600 A.D. Slightly more profiles suggest RSL rose above present during this interval and then fell but this pattern is not strong when all marsh profiles are considered. A clearer picture is evident for the high marsh profiles which show RSL remained close to present during this time interval. The Aasiaat data show a similar overall spread. Finally, the five profiles from Nanortalik all show RSL rose close to present by the 20th century and none indicate a higher than present RSL after 1750 A.D.

The use of multiple diatom profiles confirms that RSL at Sisimiut and Aasiaat slowed after c. 1600 A.D. and then remained stable close to present. The lack of absolute dating during the last 200 years does not influence this interpretation because the sedimentary sequences are continuous to the present day. Indeed, as noted above, had RSL continued to rise in these locations this would be manifest by high marshes being converted to low marshes, and low marshes to tidal flat which is not the case. The Nanortalik data show a quite distinct pattern compared with the other two sites, with long-term RSL rise persisting until at least AD 1750 and becoming stable by the latter part of the 20th century.

There are limited (in terms of record length and site distribution) tide gauge and GPS data against which to compare our salt marsh reconstructions. Fleming (2005) reviews available tide gauge data from southern Greenland and notes that the records from Aasiaat and Sisimiut are less than a decade in length (June 1997-June 1999 and September 1991-December 1999 respectively), whilst a third record from Qaqortoq (close to Nanortalik) is

also short (September 1991-December 1999). The data from Sisimiut and Qaqortoq, corrected by the removal of annual and semi-annual cycles, yield rates of RSL change of 3.4 ± 4.5 mm/a and -25.4 ± 3.3 mm/a respectively. Fleming (2005) notes that the latter rate of sea level fall is unreasonably high and cannot reflect glacio-isostatic processes. The Sisimiut record is therefore the only tide gauge data that we can compare to our salt marsh data and indicates recent RSL rise that we do not observe in the recent salt marsh data. In summary, the absence of long-term tide gauge data make independent testing of our salt marsh reconstructions with these data difficult.

GPS observations provide an alternative source of information that can be compared to our RSL records. However, they record the present-day land motion component of the RSL signal only and so a useful comparison requires information on contemporary changes in sea-surface height as well as the elastic component of vertical land motion. Furthermore, the accuracy of absolute land motion inferred via GPS is limited due to reference frame uncertainties. Given these complicating factors, we do not use these data for comparison here.

3. Discussion

3.1 Predicting present-day solid earth motions using GIA models

Relative sea-level data provide important constraints on GIA models of the GIS that are used to model Holocene and current bedrock motions. Over millennial timescales the most powerful of these are from isolation basins that provide defined age and height data on former RSL. During the late Holocene, drowned lakes provide information on the timing and pattern of RSL rise (e.g. Long et al., 2003; Long et al., 1999; Sparrenbom et al., 2006a; Sparrenbom et al., 2006b). However, there are no isolation basin data available in Greenland from the last 700 years and so GIA models assume that RSL rose at a constant rate over this interval (Tarasov and Peltier 2002; Simpson et al., 2009). Our salt marsh RSL records from west Greenland show that this is not the case and that there have been significant regional and temporal differences in the rate of RSL during this interval.

Bedrock motions predicted by ICE-5G/VM2 (Tarasov and Peltier, 2002) and Huy2 (Simpson et al., 2009) differ for our study sites, reflecting variations in earth and ice models. Both predict subsidence in central west Greenland (-1.5 to -3 mm/a (ICE-5G/VM2), 0.06 to -0.44 mm/a (Huy2)), whilst in southern Greenland the former predicts uplift (1 mm/a) and the latter subsidence (-0.73 mm/a). Subsidence is indicated by drowned isolation basins at all three

study sites and by our salt marsh data up until c. 1600 A.D. in central west Greenland and until 1750 A.D. or later in southern Greenland. During this period RSL data and GIA model predictions are broadly similar. More recently, our salt marsh records indicate stable RSL which is in conflict with the modelled bedrock motions at Aasiaat and Sisimiut.

Interpreting ice surface elevation and gravity (e.g. GRACE) survey data for recent changes in the GIS requires accurate knowledge of current bedrock motions. In principle, a GIA model tuned to predict subsidence in west Greenland during the last millennium will result in an under-estimate of present surface lowering or mass loss of the ice sheet. Our study shows that assuming constant rates of RSL change in the last millennium is not accurate and will lead to errors when using GIA models to separate the signals associated with solid earth motion and ice surface elevation or mass change.

3.2 Drivers of RSL change in Greenland during the Little Ice Age

As discussed in Section 1.2, the records from all three sites should be interpreted within the context of steadily rising RSL dominated by land subsidence. Significant departures from the observed late Holocene RSL rise could be due to a variety of processes; some that are relatively local such as changes in the GIS or changes in the adjacent ocean (e.g. steric) or due to volume changes in non-Greenland ice and the resulting RSL response at our data sites. These processes are considered quantitatively in the modelling analysis of Wake et al. (2011, this issue). In the following, we make a preliminary qualitative interpretation of the observations and hypothesize two mechanisms that would support this interpretation. The data from all three sites indicate a clear deceleration in RSL which counter-balances the background, subsidence-driven RSL rise. This is most likely due to regional mass loss causing a component sea-level fall though land uplift and sea-surface fall (the latter through associated changes in the regional gravity field).

The RSL data from Nanortalik record RSL rise throughout the period from 1300 to at least 1750 A.D. Our single high marsh diatom profile from this site shows RSL was stable during the latter part of the 20th century (Figure 2 in Supplementary Information). There is geomorphic evidence that parts of the Julianehåb ice cap and the Qassimiut ice lobe (Figure 1) retreated in many areas during the last century (Weidick et al., 2004). Therefore, the RSL record at Nanortalik likely records a combination of regional land subsidence and growth of the southern sector of the ice sheet, followed by relatively stable sea levels due, at least partly, to the contribution from local ice retreat.

The data from Sisimiut and Aasiaat record a different pattern with RSL rise up to c. 1600 A.D. followed by a slow-down, resulting in effectively no change in sea level through to the present. There is no reason to think that this slow-down is of non-Greenland origin; the regional land subsidence discussed above is a slow, steady process and the absence of a simultaneous slow-down at Nanortalik rules out a signal of dominantly eustatic origin. Moreover, modelling by Wake et al. (2011, this issue) demonstrates that other potential drivers, notably steric effects, a viscous response to possible mass loss during the Medieval Climate Anomaly and enhanced discharge from Jakobshavn Isbrae cannot, on their own, explain the RSL slow-down we observe. We therefore interpret the RSL slow-down at Aasiaat and Sisimiut after c. 1600 A.D. to be due to a sustained reduction in ice load in central west Greenland.

We now consider two possible mechanisms for such a loss of mass during the Little Ice Age when intuitively one might expect the ice sheet to be gaining mass and causing RSL to rise.

Our first hypothesis is that conditions were cold and dry in west Greenland during the LIA and that this caused a reduction in accumulation and hence ice load relative to the pre-1600 A.D. interval. There is some palaeoclimate evidence for drier, cooler and windier conditions from close to Kangerlussauq (Figure 1) from lake sediment cores and shorelines after c. 200 A.D. (Aebly and Fritz, 2009; Heggen et al., 2010). Moreover, Andersen et al. (2006) suggest a slight reduction in accumulation rates from an analysis of 5 ice cores from c. 1400 A.D. through to the late 17th century that they attribute to cold and dry conditions in the LIA.

Our second hypothesis is that temperatures were warmer than present in west Greenland after c. 1600 A.D. and that this caused sections of the ice sheet to lose mass. A review of palaeoclimate records from this period in Greenland shows that most identify a general shift to cooler conditions after c. 3000 cal yr B.P. associated with the onset of the neoglacial (Andresen et al., 2004; Bennike et al., 2010; Fredskild, 1983; Heggen et al., 2010; Kaplan et al., 2002). However, it is important to note that most records from c. 1400 A.D. onwards are poorly dated and of low resolution, certainly compared with their Canadian or European arctic equivalents (Kaufman et al., 2009). Several sedimentary records from west and south Greenland fjords record periods of increased presence of warm, Atlantic waters during the LIA, sourced from the North Atlantic (Lassen et al., 2004; Seidenkrantz et al., 2007), although the pattern is complicated, partly reflecting the complex hydrographic conditions of fjord settings with variable ocean and ice sheet influences.

Warmer than present air temperatures during the LIA in central west Greenland are compatible with the present-day climate seesaw (Van Loon and Rogers, 1978) that exists between this region and northern Europe and is related to the North Atlantic Oscillation (NAO). Changes in NAO phase drive significant changes in surface air temperature, winds, storminess and precipitation over the entire North Atlantic region (Hurrell, 1995), including Greenland (Box, 2002; Box, 2006; Hanna et al., 2008). They can also result in changes in ocean heat content and salinity, as well as sea ice cover in the Labrador Sea (Rennermalm et al., 2007). Palaeoclimate data suggest that an important shift from generally positive to more negative NAO mode occurred between c. 1300 and 1600 A.D. (Trouet et al., 2009) and this may have caused increased air and sea surface temperatures in west Greenland (see also (Mann et al., 2009)). An analogous event in the mid- 1990s resulted in a significant increase in the melt area of the southwest part of the Greenland Ice Sheet (Bhattacharya et al., 2009) as well as increased melting and accelerated discharge of tide-water glaciers (Holland et al., 2008). Interestingly, Krawczyk et al. (2010) use diatom data from a sea bed core collected from Disko Bugt to infer cool surface waters in the Roman Warm Period and the MCA and warm surface waters in the LIA. They hypothesise that these patterns reflect changes in sea ice melt and meltwater flux from the GIS; during the warm MCA they suggest increased GIS and sea ice melt caused greater meltwater flux and the opposite during the LIA. An alternative hypothesis for these trends is that they in fact record changes in air temperatures as expected under the climate seesaw described above. To test these hypotheses further requires the generation of new quantitative air temperature records from sites adjacent to the ice sheet margin in west Greenland.

4. Conclusions

We constrain relative sea-level changes and vertical land motions at three sites in west Greenland during the last 700 years using newly collected contemporary and fossil salt marsh data. Our conclusions are:

1. At Aasiaat and Sisimiut, MTL rises from c. -0.80 ± 0.20 m at 1300 A.D. to c. -0.10 m ± 0.20 m at c. 1600 A.D. and then stabilised until present. Diatom data from multiple sediment profiles at each site record the initial rapid submergence of the deepest samples, formed prior to c. 1600 A.D., with negligible RSL change in the period between c. 1600 A.D. and present. At Nanortalik, in south Greenland, we record a continuous rise in RSL from c. -1.40 ± 0.20 m at c. 1450 A.D. to -0.30 ± 0.25 m at c.1750 A.D., with stable RSL during at least the latter part of the 20th century.

2. RSL rise due to crustal subsidence was ongoing at all sites between c. 1300 to 1600 A.D., after which RSL slowed at Sisimiut and Aasiaat. Since c. 1600 A.D., rates of RSL have remained close to zero at these sites. The slow-down at c. 1600 A.D. is not observed at Nanortalik and therefore it reflects a regional change in RSL in central west Greenland at this time.

3. The 1600 A.D. RSL slow-down is the largest signal evident in the observations and suggests a loss of ice mass during this part of the Little Ice Age. This is surprising since a large body of previous research suggests that the ice sheet was gaining mass during this interval. Wake et al. (this issue) provide a modelling-based interpretation of the RSL data.

4. The current generation of GIA models tuned to fit millennial-scale RSL data do not capture the shorter-term variability resolved using the salt marsh records. These models therefore over-predict present-day land subsidence in western central Greenland and so their use in the interpretation of geodetic observations for contemporary ice mass changes will lead to a bias.

5. Future research priorities include additional RSL constraints, especially between Sisimiut and Nanortalik to constrain the pattern of RSL in this region during the LIA, and well-dated quantitative palaeoclimate reconstructions from sites close to the ice sheet margin in west Greenland to determine whether air temperatures were warmer or cooler than present during the LIA.

Acknowledgements

The research was completed as part of NERC Grant NE/C519311/1. We thank the NERC Radiocarbon Laboratory and SUERC AMS Laboratory in East Kilbride, Scotland for support with the radiocarbon dating under award numbers 1234.0407, 1239.1007 and 1319.1008 and in particular the meticulous work of Margaret Currie and Philippa Ascough. Will Todd was a great help in the field during field seasons to Nanortalik and Sisimiut, Katie Stokes assisted in the laboratory work, and we thank Palle Bo Nielsen for advice regarding tidal matters. The comments of two anonymous referees improved the paper, which is a contribution to PALSEA, the INQUA Commission on Coastal and Marine Processes, to IGCP588 and also to the APEX (Arctic Palaeoclimate and Its Extremes) programme.

Supplementary data

Supplementary data for this manuscript are provided to support this paper.

References

Aebly, F.A., Fritz, S.C., 2009. Palaeohydrology of Kangerlussuaq (Sondre Stromfjord), West Greenland during the last ~8000 years. Holocene 19, 91-104.

Andersen, K.K., Ditlevsen, P.D., Rasmussen, S.O., Clausen, H.B., Vinther, B.M., Johnsen, S.J., Steffensen, J.P., 2006. Retrieving a common accumulation record from Greenland ice cores for the past 1800 years. J. Geophys. Res.-Atmos. 111, D18106.

Andresen, C.S., Björck, S., Bennike, O., Bond, G., 2004. Holocene climate changes in southern Greenland: evidence from lake sediments. Journal of Quaternary Science 19, 783-795.

Bennike, O., Anderson, N.J., McGowan, S., 2010. Holocene palaeoecology of southwest Greenland inferred from macrofossils in sediments of an oligosaline lake. Journal of Paleolimnology 43, 787-798.

Bennike, O., Sparrenbom, C.J., 2007. Dating of the Narssarssuaq stade in southern Greenland. Holocene 17, 279-282.

Bhattacharya, I., Jezek, K.C., Wang, L., Liu, H.X., 2009. Surface melt area variability of the Greenland ice sheet: 1979-2008. Geophys. Res. Lett. 36, L20502.

Box, J.E., 2002. Survey of Greenland instrumental temperature records: 1873-2001. International Journal of Climatology 22, 1829-1847.

Box, J.E., 2006. Greenland ice sheet surface mass balance variability: 1991-2003. Annals of Glaciology 42, 42A142.

Briner, J.P., Stewart, H.A.M., Young, N.E., Philipps, W., Losee, S., 2010. Using proglacial-threshold lakes to constrain fluctuations of the Jakobshavn Isbrae ice margin, western Greenland, during the Holocene. Quaternary Science Reviews 29, 3861-3874.

Bronk Ramsey, C., 1995. Radiocarbon calibration and analysis of stratigraphy: the OxCal program. Radiocarbon 37, 425-430.

Bronk Ramsey, C., 2001. Development of the radiocarbon calibration program. Radiocarbon 43, 355-363.

Christiansen, H.H., 1998. 'Little Ice Age' nivation activity in northeast Greenland. Holocene 8, 719-728.

Craig, H., 1957. Isotopic standards for carbon and oxygen and correction factors for mass-spectrometric analysis of carbon dioxide. Geochim. Cosmochim. Acta 12, 133-149.

Dahl-Jensen, D., Mosegaard, K., Gundestrup, N., Clow, G.D., Johnsen, S.J., Hansen, A.W., Balling, N., 1998. Past temperatures directly from the Greenland Ice Sheet. Science 282, 268-271.

Dawson, A.G., Hickey, K., Mayewski, P.A., Nesje, A., 2007. Greenland (GISP2) ice core and historical indicators of complex North Atlantic climate changes during the fourteenth century. Holocene 17, 427-434.

Dietrich, R., Maas, H.G., Baessler, M., Ruelke, A., Richter, A., Schwalbe, E., Westfeld, P., 2007. Jakobshavn Isbrae, West Greenland: Flow velocities and tidal interaction of the front area from 2004 field observations. Journal of Geophysical Research-Earth Surface 112, F03S21.

Dietrich, R., Rulke, A., Scheinert, M., 2005. Present-day vertical crustal deformations in West Greenland from repeated GPS observations. Geophys. J. Int. 163, 865-874.

Fleming, K., Wunsch, J., Lambeck, K., 2005. Glacial-isostatic contributions to present-day sea-level change around Greenland. Department 1 Geodesy and Remote Sensing, GeoForschungsZentrum, Potsdam, Germany, p. 21.

Forman, S.L., Marin, L., van der Veen, C., Tremper, C., Csatho, B., 2007. Little ice age and neoglacial landforms at the Inland Ice margin, Isunguata Sermia, Kangerlussuaq, west Greenland. Boreas 36, 341-351.

Fredskild, B., 1983. The Holocene vegetational development of the Godhåbsfjord area, west Greenland. Meddelelser om Grønland Geoscience 10, 1-27.

Funder, S., Hansen, L., 1996. The Greenland ice sheet - a model for its culmination and decay during and after the last glacial maximum. Bulletin of the Geological Society of Denmark 42, 137-152.

Grove, J.M., 1988. The Little Ice Age. Methuen, London.

Hall, B.L., Baroni, C., Denton, G.H., 2007. The most extensive Holocene advance in the Stauning Alper, East Greenland, occurred in the Little Ice Age. Polar Research 27, 128-134.

Hanna, E., Huybrechts, P., Steffen, K., Cappelen, J., Huff, R., Shuman, C., Irvine-Fynn, T., Wise, S., Griffiths, M., 2008. Increased runoff from melt from the Greenland Ice Sheet: A response to global warming. Journal of Climate 21, 331-341.

Heggen, M.P., Birks, H.H., Anderson, N.J., 2010. Long-term ecosystem dynamics of a small lake and its catchment in west Greenland. The Holocene 20, 1207-1222.

Hoffmann, G., Jouzel, J., Johnsen, S.J., 2001. Deuterium excess record from central Greenland over the last millennium: Hints of a North Atlantic signal during the Little Ice Age. Journal of Geophysical Research 106, 14265-14274.

Holland, D.M., Thomas, R.H., De Young, B., Ribergaard, M.H., Lyberth, B., 2008. Acceleration of Jakobshavn Isbrae triggered by warm subsurface ocean waters. Nature Geoscience 1, 659-664.

Hurrell, J.W., 1995. Decadal trends in the North Atlantic Oscillation: Regional temperatures and precipitation. Science 269, 676-679.

Johnsen, S.J., Dahl-Jensen, D., Gundestrup, N., Steffensen, J.P., Clausen, H.B., Miller, H., Masson-Delmotte, V., Sveinbjornsdottir, A.E., White, J., 2001. Oxygen isotope and palaeotemperature records from six Greenland ice-core stations: Camp Century, Dye-3, GRIP, GISP2, Renland and NorthGRIP. Journal of Quaternary Science 16, 299-307.

Kaplan, M.R., Wolfe, A.P., Miller, G.H., 2002. Holocene environmental variability in southern Greenland inferred from lake sediments. Quaternary Research 58, 149-159.

Kaufman, D.S., Schneider, D.P., McKay, N.P., Ammann, C.M., Bradley, R.S., Briffa, K.R., Miller, G.H., Otto-Bliesner, B.L., Overpeck, J.T., Vinther, B.M., 2009. Recent warming reverses long-term Arctic cooling. Science 325, 1236-1239.

Kelly, M.A., Lowell, T.V., 2009. Fluctuations of local glaciers in Greenland during latest Pleistocene and Holocene time. Quaternary Science Reviews 28, 2088-2106.

Khan, S.A., Liu, L., Wahr, J., Howat, I., Joughin, I., van Dam, T., Fleming, K., 2010. GPS measurements of crustal uplift near Jakobshavn Isbrae due to glacial ice mass loss. J. Geophys. Res.-Solid Earth 115, B09405.

Khan, S.A., Wahr, J., Stearns, L.A., Hamilton, G.S., van Dam, T., Larson, K.M., Francis, O., 2007. Elastic uplift in southeast Greenland due to rapid ice mass loss. Geophys. Res. Lett. 34, L21701.

Krawczyk, D., Witkowski, A., Moros, M., Lloyd, J., Kuijpers, A., Kierzek, A., 2010. Late-Holocene diatom-inferred reconstruction of temperature variations of the West Greenland Current from Disko Bugt, central West Greenland. Holocene 20, 659-666.

Kreutz, K.J., Mayewski, P.A., Meeker, L.D., Twickler, M.S., Whitlow, S.I., Pittalwala, I.I., 1997. Bipolar changes in atmospheric circulation during the Little Ice Age. Science, 1294-1296.

Lamb, H.H., 1977. Climate: Present, Past and Future. Volume 2: Climatic History and the Future. Methuen, London.

Lambeck, K., Anzidei, M., Antonioli, F., Benini, A., Esposito, A., 2004. Sea level in Roman time in the Central Mediterranean and implications for recent change. Earth Planet. Sci. Lett. 224, 563-575.

Lassen, S.J., Kuijpers, A., Kunzendorf, H., Hoffman-Wieck, G., Mikkelsen, N., Konradi, P., 2004. Late-Holocene Atlantic bottom-water variability in Igaliku Fjord, South Greenland, reconstructed from foraminifera faunas. The Holocene 14, 165-171.

Long, A.J., Roberts, D.H., Dawson, S., 2006. Early Holocene history of the West Greenland Ice Sheet and the GH-8.2 event. Quaternary Science Reviews 25, 904-922.

Long, A.J., Roberts, D.H., Rasch, M., 2003. New observations on the relative sea level and deglacial history of Greenland from Innaarsuit, Disko Bugt. Quaternary Research 60, 162-171.

Long, A.J., Roberts, D.H., Simpson, M.J.R., Dawson, S., Milne, G.A., Huybrechts, P., 2008. Late Weichselian relative sea-level changes and ice sheet history in southeast Greenland. Earth Planet. Sci. Lett. 272, 8-18.

Long, A.J., Roberts, D.H., Wright, M.R., 1999. Isolation basin stratigraphy and Holocene relative sea-level change on Arveprinsen Ejland, Disko Bugt, West Greenland. Journal of Quaternary Science 14, 323-345.

Long, A.J., Woodroffe, S.A., Milne, G.A., Bryant, C.L., Wake, L.M., 2010. Relative sea-level change in West Greenland during the last millennium. Quaternary Science Reviews 29, 367-383.

Mann, M.E., Zhang, Z.H., Rutherford, S., Bradley, R.S., Hughes, M.K., Shindell, D., Ammann, C., Faluvegi, G., Ni, F.B., 2009. Global signatures and dynamical origins of the Little Ice Age and Medieval Climate Anomaly. Science 326, 1256-1260.

Mayewski, P.A., Meeker, L.D., Morrison, M.C., Twickler, M.S., Whitlow, S.I., Ferland, K.K., Meese, D.A., Legrand, M.R., Steffensen, J.P., 1993. Greenland ice core signal characteristics - an expanded view of climate-change. J. Geophys. Res.-Atmos. 98, 12839-12847.

Ogilvie, A.E.J., Jonsson, T., 2001. Little Ice Age research: a perspective from Iceland. Climatic Change 48, 9-52.

Rennermalm, A.K., Wood, E.F., Weaver, A.J., Eby, M., Dery, S.J., 2007. Relative sensitivity of the Atlantic meridional overturning circulation to river discharge into Hudson Bay and the Arctic Ocean. Journal of Geophysical Research-Biogeosciences 112, G04S48.

Seidenkrantz, M.-S., Aagaard-Sørensen, S., Sulsbrück, H., Kuijpers, A., Jensen, K.G., Kunzendorf, H., 2007. Hydrography and climate of the last 4400 years in a SW Greenland fjord: implications for Labrador Sea palaeoceanography. The Holocene 17, 387-401.

Simpson, M.J.R., Milne, G.A., Huybrechts, P., Long, A.J., 2009. Calibrating a glaciological model of the Greenland ice sheet from the last glacial maximum to present-day using field observations of relative sea level and ice extent. Quaternary Science Reviews 28, 1631-1657.

Sparrenbom, C., Lambeck, K., Bennike, O., Björck, S., 2006a. Holocene relative sea-level changes in the Qaqortoq area, southern Greenland. Boreas 35, 171-187.

Sparrenbom, C.J., Bennike, O., Björck, S., Lambeck, K., 2006b. Relative sea-level changes since 15 000 cal. yr BP in the Nanortalik area, Southern Greenland. Journal of Quaternary Science 21, 29-48.

Trouet, V., Esper, J., Graham, N.E., Baker, A., Scourse, J.D., Frank, D.C., 2009. Persistent positive North Atlantic Oscillation mode dominated the Medieval Climate Anomaly. Science 324, 78-80.

Van Loon, H., Rogers, J.C., 1978. The seesaw in winter temperatures between Greenland and Northern Europe: Part I. General description. Monthly Weather Review 106, 296-310.

Weidick, A., 1972. Holocene shore-lines and glacial stages in Greenland - an attempt at correlation. Grønlands Geologiske Undersøgelse 41, 1-39.

Weidick, A., Bennike, O., 2007. Quaternary glaciation history and glaciology of Jakobshavn Isbrae and the Disko Bugt region, West Greenland: a review. Geological Survey of Denmark and Greenland Bulletin 14, 1-78.

Weidick, A., Kelly, M., Bennike, O., 2004. Late Quaternary development of the southern sector of the Greenland Ice Sheet, with particular reference to the Qassimiut lobe. Boreas 33, 284-299.

Woodroffe, S.A., Long, A.J., 2009. Salt marshes as archives of recent relative sea-level change in West Greenland. Quaternary Science Reviews 28, 1750-1761.

Woodroffe, S.A., Long, A.J., 2010. Reconstructing recent relative sea-level changes in West Greenland: local diatom-based transfer functions are superior to regional models. Quaternary International 221, 91-103.

List of figures

Figure 1 Location map showing sites referred to in the text.

Figure 2 a) Photograph of a salt marsh at Nanortalik showing the generalised vegetation zones and the average elevation of the zone boundaries across two marshes surveyed in this area. b) Photograph showing the typical salt marsh stratigraphy at Nanortalik.

Figure 3 Reconstructed trend in MTL at the three study sites using the transfer function (a) and visual assessment (b) methods. Height and age errors are defined in Table 2 and in supplementary information.

Figure 4 Palaeomarsh surface elevation reconstructions using a transfer function for 1 cm samples from cores from Sisimiut (Long et al., 2010), Aasiaat and using visual assessment for samples from cores from Nanortalik. Sedimentation rates are assumed to be constant between the youngest radiocarbon dated level and the surface in each core to produce a chronology. Cores from

current low and high marsh locations are labelled. Typical vertical errors (not shown) are ±0.20 m.

List of Tables

Table 1 Meteorological and tidal data for the study areas.

	Annual mean temp (1961-1990) ºC	Mean winter temp (1961-1990) ºC	Mean summer temp (1961-1990) ºC	Tidal range (m)	Height of Mean High Water of Neap Tides (MHWNT) above MTL (m)	Height of Mean High Water of Spring Tides (MHWST) above MTL (m)	Height of Highest Astronomical Tide (HAT) above MTL (m)
Aasiaat	-4.9	-13.0	4.6	2.86	+0.42	+0.93	+1.43
Sisimiut	-3.9	-12.3	5.3	4.66	+0.71	+1.62	+2.33
Nanortalik	0.6	-5.0	6.5	3.02	+0.51	+1.26	+1.51

Table 2 Radiocarbon dates from the study areas. $\delta^{13}C$ values were measured using a dual-inlet mass spectrometer with a multiple ion beam collection facility (VG OPTIMA) to correct ^{14}C data to –25 ‰ $\delta^{13}C_{VPDB}$. Starred $\delta^{13}C$ values indicate samples containing ≤300 µg C, which required AMS analysis at low current. The starred $\delta^{13}C$ values were calculated from $\delta^{13}C/^{12}C$ ratios measured during AMS ^{14}C determination and by comparison to Craig (1957) $\delta^{13}C/^{12}C$ values for PDB. These values are not necessarily representative of the $\delta^{13}C$ in the original sample material.

Sample code and depth below surface (cm)	Laboratory code	Material dated	Sample elevation (m MTL)	VA RSL recon-struction and error (m MTL)	TF RSL recon-struction and error (m MTL)	Sample weight (mg)	$\delta^{13}C_{VPDB}$ ‰ ± 0.1	Conventional radiocarbon age (years BP ± 1 σ)	Age range (cal. yrs BP, % in brackets)	Age range (cal. yrs AD, range as previous column)
Nanortalik										
IG1-S1-5 (4-5 cm)	SUERC-21173	*Empetrum nigrum* seeds and Cyperaceae seeds	1.67	0.06 ± 0.10	0.21 ± 0.25	1.3	-29.9*	Modern	Modern	Modern
IG1-S1-3 (10-11 cm)	SUERC-23836	*Empetrum nigrum* seeds and Cyperaceae seeds	1.43	-0.28 ± 0.11	0.78 ± 0.28	2.6	-25.7	196 ± 37	307 – 137 (73.3%)	1643-1813
IG1-S1-3 (10-11 cm)	SUERC-21172	*Empetrum nigrum* seeds and Cyperaceae seeds	1.43	-0.28 ± 0.11	0.78 ± 0.28	2.5	-20.9*	391 ± 36	512-318 (95 %) (date rejected as outlier)	1557-1632
IG1-S1-2 (12-13 cm)	SUERC-20110	*Empetrum nigrum* seeds	1.32	-0.29 ± 0.11	-0.17 ± 0.24	1.4	-24.1	160 ± 35	286 – 124 (62.9 %)	1664-1826
IG1-S1-1 (16-17 cm)	SUERC-27678	*Empetrum nigrum* seeds	1.22	-0.32 ± 0.04	0.31 ± 0.25	6.1	-24.4	170 ± 37	295 – 124 (65.8 %)	1655-1826
IG1-N2-4 (13-14 cm)	SUERC-19494	*Empetrum nigrum* seeds	1.01	-0.40 ± 0.12	-0.48 ± 0.26	3.3	-24.3	174 ± 37	298 – 131 (67.1 %)	1652-1819
IG1-N2-3 (13-14 cm)	SUERC-20021	*Empetrum nigrum* seeds	0.90	-0.54 ± 0.12	-0.60 ± 0.28	1.2	-24.1*	210 ± 35	310 – 138 (78.5 %)	1640-1812
IG1-N2-1 (18-19 cm)	SUERC-19493	*Empetrum nigrum* seeds and leaves and	0.73	-0.83 ± 0.07	-0.66 ± 0.26	1.8	-24.3	251 ± 37	435 – 268 (67.7 %)	1515-1682

Sample code and depth below surface (cm)	Laboratory code	Material dated	Sample elevation (m MTL)	VA RSL recon-struction and error (m MTL)	TF RSL recon-struction and error (m MTL)	Sample weight (mg)	$\delta^{13}C_{VPDB}$ ‰ ± 0.1	Conventional radiocarbon age (years BP ± 1 σ)	Age range (cal. yrs BP, % in brackets)	Age range (cal. yrs AD, range as previous column)
		Cyperaceae seeds								
IG1-S2-1 (9-10 cm)	SUERC-27936	Cyperaceae seeds	0.27	-1.44 ± 0.21	-0.25 ± 0.25	1.9	-28.2*	436 ± 39	540 – 429 (87.9 %)	1410-1521
IG1-N1-3 (17-18 cm)	SUERC-20972	*Empetrum nigrum* seeds and Cyperaceae seeds	0.25	-1.08 ± 0.21	-1.47 ± 0.26	3.1	-25.1	293 ± 35	466 – 286 (95 %)	1484-1664
IG1-N1-2 (16-17 cm)	SUERC-20971	*Empetrum nigrum* seeds	0.05	-1.28 ± 0.21	-1.72 ± 0.25	6.2	-25.0	334 ± 37	484 – 307 (95 %)	1466-1643
Aasiaat										
A06/M2/1 (2-3 cm)	SUERC-17058	*Empetrum nigrum* seeds and leaves and Cyperaceae seeds	1.64	0.01 ± 0.16	0.08 ± 0.17	7.0	-26.2	337 ± 36	484-308	1466-1642
T08/M2/3 (3-4 cm)	SUERC-24324 & 24325	*Empetrum nigrum* seeds and Cyperaceae seeds	1.64	-0.16 ± 0.11	-0.03 ± 0.16	2.9 2.6	-26.1 -26.1	Modern Modern	Modern Modern	Modern Modern
A06/M2/2 (7-8 cm)	SUERC-17059	*Empetrum nigrum* seeds and Cyperaceae seeds	1.52	0.00 ± 0.17	-0.06 ± 0.17	8.3	-26.2	259 ± 35	454-271 (77 %)	1496-1679

Sample code and depth below surface (cm)	Laboratory code	Material dated	Sample elevation (m MTL)	VA RSL recon-struction and error (m MTL)	TF RSL recon-struction and error (m MTL)	Sample weight (mg)	$\delta^{13}C_{VPDB}$ ‰ ± 0.1	Conventional radiocarbon age (years BP ± 1 σ)	Age range (cal. yrs BP, % in brackets)	Age range (cal. yrs AD, range as previous column)
A06/M2/3 (6-7 cm)	SUERC-17063	*Empetrum nigrum* seeds and Cyperaceae seeds	1.43	0.00 ± 0.07	-0.05 ± 0.19	1.0	-26.9	332 ± 36	482-307	1468-1643
A06/M1/4 (5-6 cm)	SUERC-17064	*Empetrum nigrum* seeds and leaves and Cyperaceae seeds	1.39	-0.41 ± 0.11	-0.22 ± 0.17	10.0	-27.5	337 ± 35	483-308	1467-1642
T08/M2/1 (4-5 cm)	SUERC-24326 & 24330	*Empetrum nigrum* seeds and Cyperaceae seeds	1.38	-0.25 ± 0.07	-0.26 ± 0.16	2.9 2.5	-27.0 -27.0	154 ± 33 94 ± 33	285-59 (78.1 %) 268-15	1665-1891 1682-1935
A06/M1/5 (9-10 cm)	SUERC-17069	*Empetrum nigrum* seeds and leaves and Cyperaceae seeds	1.23	-0.17 ± 0.21	0.30 ± 0.17	14.0	-26.6	284 ± 35	460-284 (93 %)	1490-1666
A06/M2/6 (6-7 cm)	SUERC-16537	*Empetrum nigrum* seeds and Cyperaceae seeds	1.13	-0.37 ± 0.21	-0.29 ± 0.16	2.0	-29.3	490 ± 35	555-496 (93 %)	1395-1454
T08/M1/7 (2-3 cm)	SUERC-24332	*Empetrum nigrum* seeds,	1.04	-0.16 ± 0.21	-0.30 ± 0.18	1.5	-26.1	152 ± 35	285-59 (78.3 %)	1665-1891

Sample code and depth below surface (cm)	Laboratory code	Material dated	Sample elevation (m MTL)	VA RSL recon-struction and error (m MTL)	TF RSL recon-struction and error (m MTL)	Sample weight (mg)	$\delta^{13}C_{VPDB}$ ‰ ± 0.1	Conventional radiocarbon age (years BP ± 1 σ)	Age range (cal. yrs BP, % in brackets)	Age range (cal. yrs AD, range as previous column)
		Cyperaceae seeds and *Vaccinium uliginosum* leaves								
A06/M2/7 (7-8 cm)	SUERC-17070	*Empetrum nigrum* seeds and Cyperaceae seeds	1.03	-0.67 ± 0.13	-0.59 ± 0.16	4.7	-26.5	505 ± 36	558-501 (87.5 %)	1392-1449
T08/M4/2 (15-16 cm)	SUERC-24333	Cyperaceae seeds and *Vaccinium uliginosum* leaves	0.93	-0.87 ± 0.20	-0.73 ± 0.16	1.6	-25.0	277 ± 35	459-282 (91 %)	1491-1668
T08/M1/4 (3-4 cm)	SUERC-24331	Cyperaceae seeds and *Vaccinium uliginosum* leaves	0.63	-0.57 ± 0.14	-0.51 ± 0.18	3.3	-25.5	402 ± 35	516-427 (72.4 %)	1434-1523
T08/M3/2 (6-7 cm)	SUERC-24323	*Empetrum nigrum* seeds and Cyperaceae seeds	0.54	-0.88 ± 0.14	-0.72 ± 0.17	1.0	-25.1	577 ± 35	652-528	1298-1422
T08/M1/3 (3-4 cm)	SUERC-24322	*Empetrum nigrum* seeds and Cyperaceae	0.52	-0.68 ± 0.14	-0.74 ± 0.17	2.4	-25.6	618 ± 35	660-546	1290-1404

Sample code and depth below surface (cm)	Laboratory code	Material dated	Sample elevation (m MTL)	VA RSL recon-struction and error (m MTL)	TF RSL recon-struction and error (m MTL)	Sample weight (mg)	$\delta^{13}C_{VPDB}$ ‰ ± 0.1	Conventional radiocarbon age (years BP ± 1 σ)	Age range (cal. yrs BP, % in brackets)	Age range (cal. yrs AD, range as previous column)
		seeds								
T08/M3/1 (8-9 cm)	SUERC-24320	*Empetrum nigrum* seeds and Cyperaceae seeds	0.49	-0.93 ± 0.14	-0.82 ± 0.17	2.4	-24.9	656 ± 35	674-555	1276-1395
T08/M1/1 (6-7 cm)	SUERC-24321	*Empetrum nigrum* seeds and Cyperaceae seeds	0.33	-0.87 ± 0.14	-0.90 ± 0.17	2.0	-24.8	514 ± 35	559-503 (83.2 %)	1391-1447

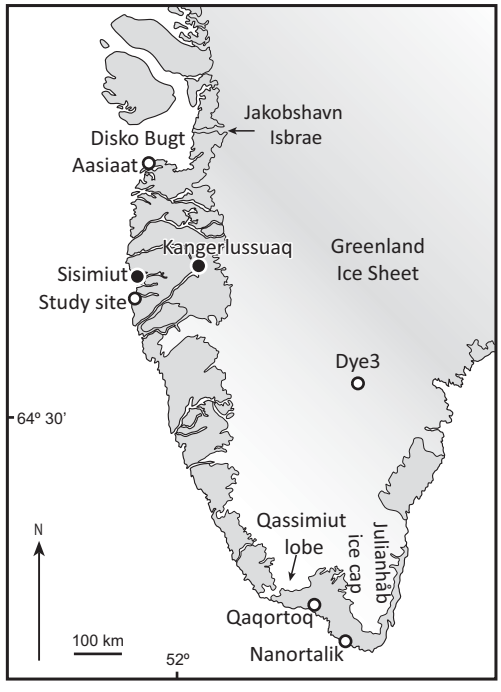
Jakobshavn
Isbrae
Disko Bugt
Aasiaat
Kangerlussuaq
Greenland
Ice Sheet
Sisimiut
Study site
Dye3
64° 30'
Qassimiut
lobe
ice cap
Julianhåb
N
Qaqortoq
100 km
Nanortalik
52°

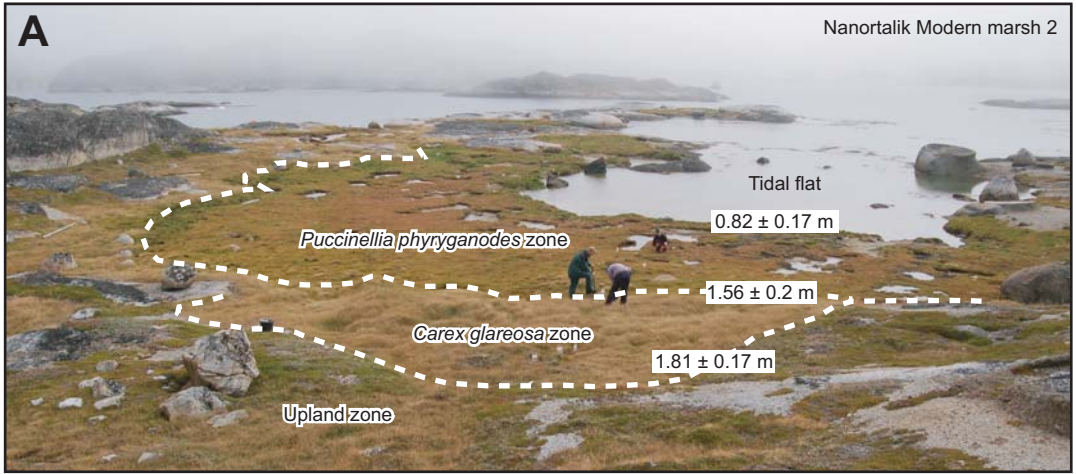
A
Nanortalik Modern marsh 2
Tidal flat
0.82 ± 0.17 m
Puccinellia phyryganodes zone
1.56 ± 0.2 m
Carex glareosa zone
1.81 ± 0.17 m
Upland zone


B

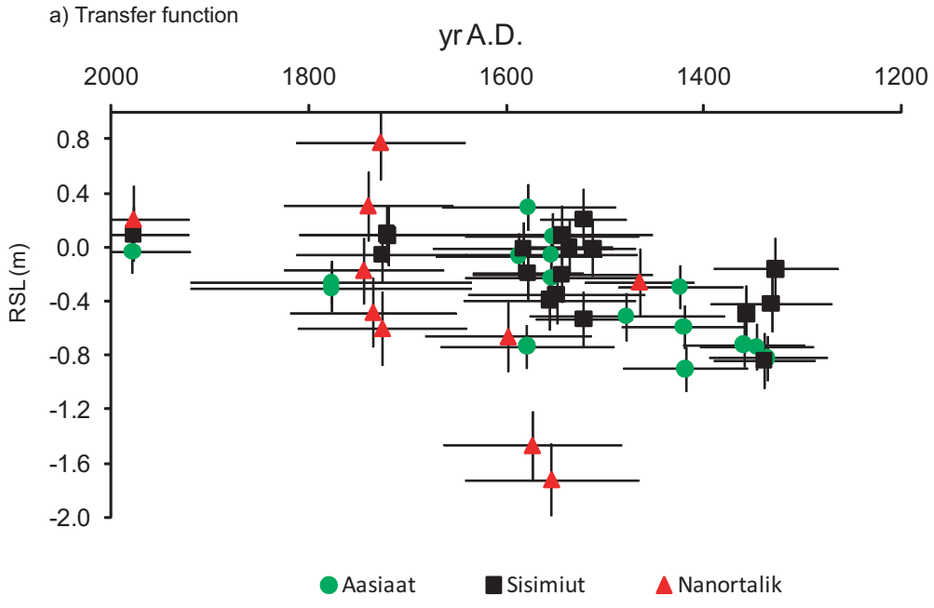
a) Transfer function
yr A.D.
2000
1800
1600
1400
1200
0.8
0.4
0.0
-0.4
-0.8
-1.2
-1.6
-2.0
RSL (m)
Aasiaat
Sisimiut
Nanortalik

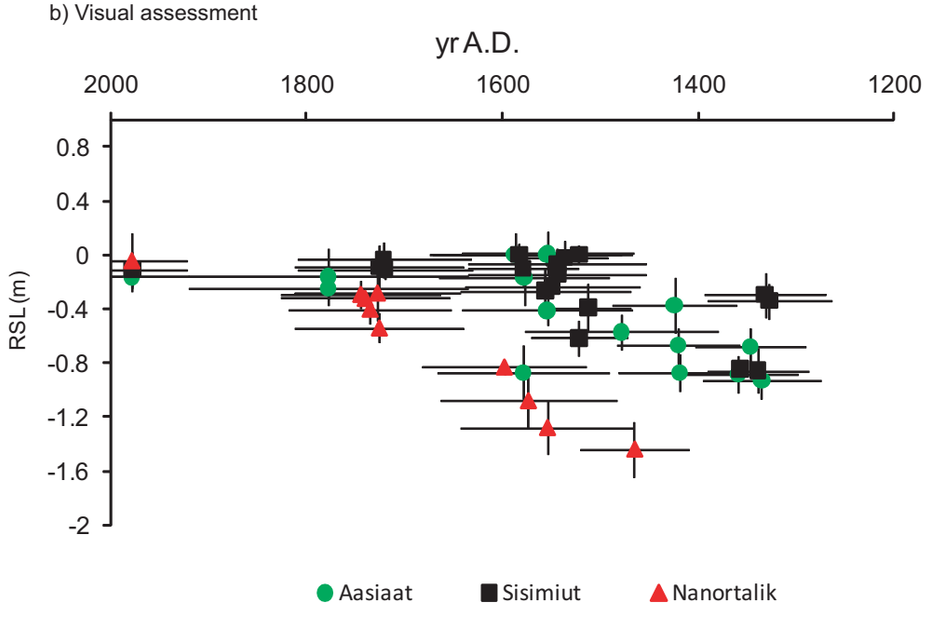
b) Visual assessment
yr A.D.
2000
1800
1600
1400
1200
0.8
0.4
0
-0.4
-0.8
-1.2
-1.6
-2
RSL (m)
Aasiaat
Sisimiut
Nanortalik

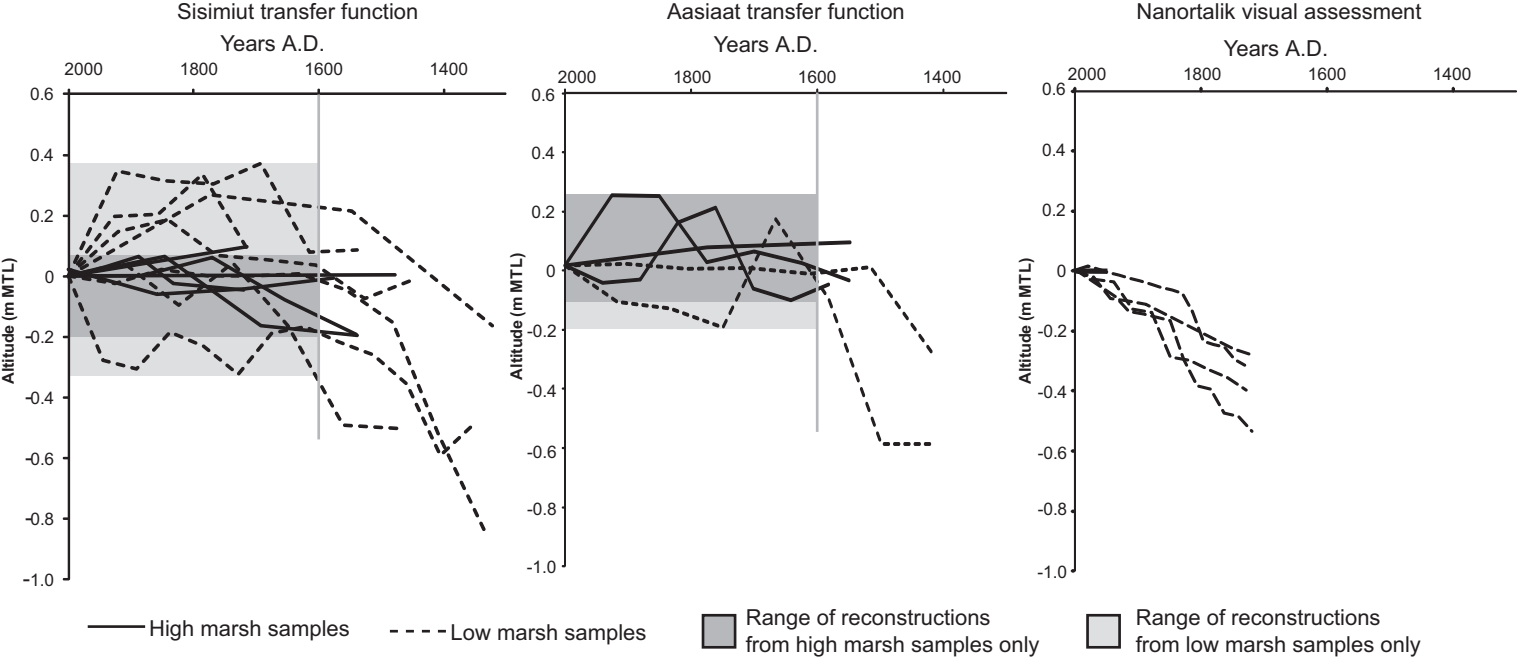
Sisimiut transfer function
Aasiaat transfer function
Nanortalik visual assessment
Years A.D.
2000
1800
1600
1400
0.6
0.4
0.2
0
-0.2
-0.4
-0.6
-0.8
-1.0
Altitude (m MTL)
High marsh samples
Low marsh samples
Range of reconstructions from high marsh samples only
Range of reconstructions from low marsh samples only

Supplementary Information

In this supplementary information we provide details of the salt marsh lithology, contemporary and fossil diatoms and radiocarbon dates from our three study sites.

1. Nanortalik

The sample sites at Nanortalik are located c. 28 km SW of Nanortalik town (Figure S1). We collected modern diatom samples from two marshes (Modern marsh 1 and Modern marsh 2, Figure S2) and fossil samples from the north and south side of the studied embayment.

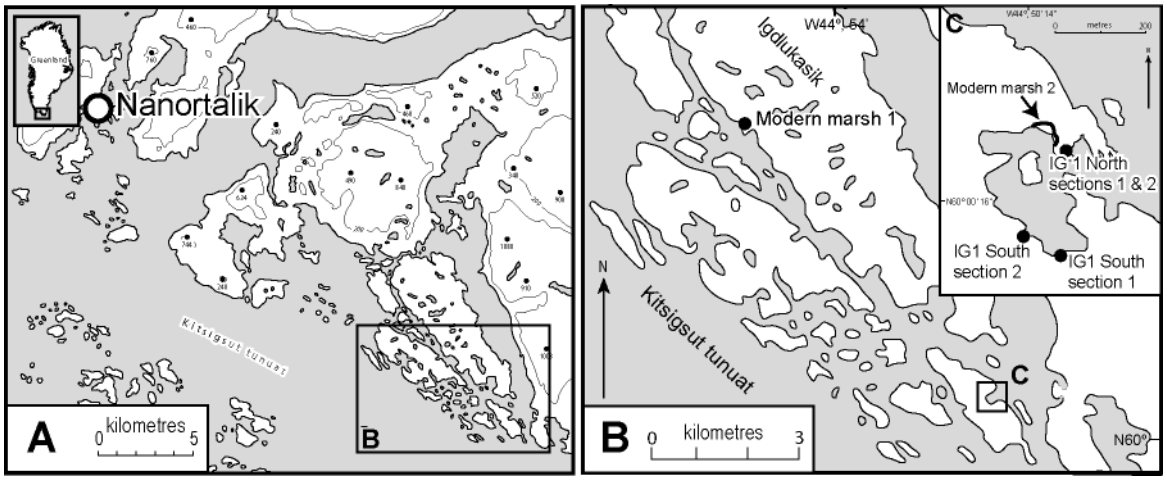

Figure S1. Location map of Nanortalik area.

1.1 Contemporary data

We collected contemporary data from two salt marshes in August 2007, examining 59 samples for diatom analysis collected from between 1.90 m and -0.6 m MTL (Figure S2). The high marsh assemblage contains high frequencies of *Nitzschia sigma*, *Hantzschia amphioxys*, *Pinnularia intermedia* and *Pinnularia microstauron*. A more diverse assemblage characterises the low marsh, with *Navicula salinarum*, *Navicula peregrina* and *Navicula cincta* dominant. A tidal flat assemblage is dominated by *Fragilariforma virescens* and lesser frequencies of *Cocconeis scutellum*, *Achnanthes delicatula*, *Navicula salinarum* and *Martyana martyi*. %LOI generally declines with elevation across the high and low marsh, falling from values of c. 80-50% between HAT and MHWST to <10% on the tidal flat. Grain size data show the marshes are predominantly sand with some silt.

Detrended Canonical Correspondence Analysis (DCCA) (using CANOCO, release 4.51, ter Braak and Šmilauer, 1998; 2003) show a unimodal taxon-environment response model applies for the TFs developed at Nanortalik (and elsewhere) in this paper (Birks, 1995). To allow comparison with our other study sites, we use the unimodal technique Weighted Averaging Partial Least Squares (WA-PLS) in the C2 program, version 1.5 for all transfer function regression and calibration (ter Braak and Juggins, 1993; Birks, 1995; Juggins, 2007). All other statistical methods used here are as described in Woodroffe and Long (2009; 2010).

Our preferred training set is a 'pruned model' which excludes species that occur in only one sample and also samples that have an absolute residual greater than one quarter of the elevation range of the training set (Figure S3). The prediction statistics are similar to the local transfer function models that we developed from salt marshes at Sisimiut and Aasiaat (Table S1).

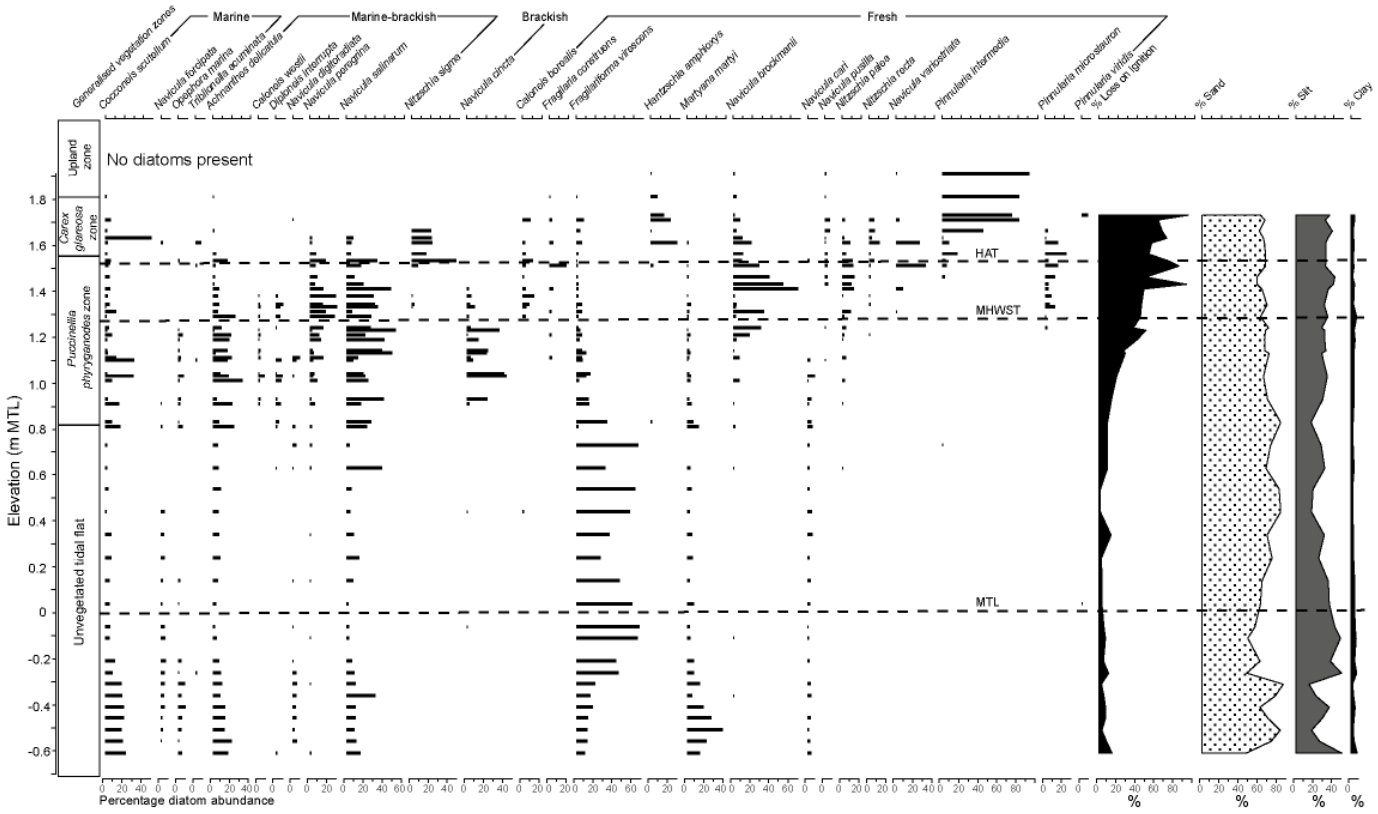

Figure S2. Contemporary diatom data and generalised vegetation zones for the Nanortalik salt marshes. Data are expressed as a % Total Diatom Valves (%TDV). Only data >5% TDV are shown.

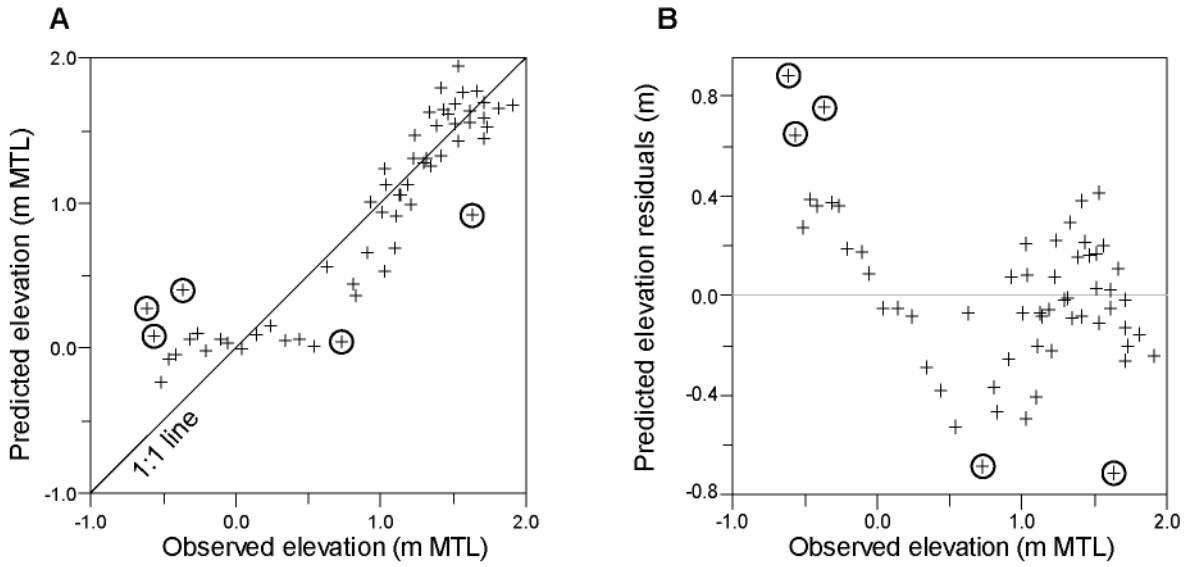

Figure S3. a) Observed versus predicted elevation for the full dataset from Nanortalik (59 samples, WA PLS component 2) with the samples removed in the final 'pruned model' circled. b) residuals associated with the full dataset, sampled removed from the final 'pruned model' highlighted.

Table S1.

Model description and elevation range	Bootstrapped RMSEP (m)	Bootstrapped r^2
Pruned model (54 samples, 2.42 m range, -0.51 m MTL to +1.91 m MTL)	Component 1 - 0.31 **Component 2 – 0.25** Component 3 – 0.22	0.81 **0.88** 0.92

Transfer function model details.

1.2 Fossil data

We collected fossil salt marsh sediments a small tidal embayment on an island to the south of Igdlukasik (Figure S1). Much of the embayment dries out at low tide to expose tidal flats with fringing salt marsh. Freshwater peat overlies bedrock at each of the four sample locations and is in turn overlain by salt marsh sediments. We collected sediment profiles that contain the transition from the freshwater peat to the salt marsh sediment at 10 locations Dated samples are from the north sections

(IG1/N1/2, IG1/N1/3, IG1/N2/1, IG1/N2/3, IG1/N2/4) and the south sections (IG1/S1/2, IG1/S1/3, IG1/S1/5 IG1/S2/1) (Figures S4, S5 and Table S2).

IG1-N2-3

The lithology is a dark brown humified peat overlain by a salt marsh peat that shows a declining %LOI and increasing sand content up-profile (Figure S5A). The diatoms show increased salinity as frequencies of *Pinnularia microstauron* decline while those of *Diploneis interrupta, N. peregrina* and *Navicula cincta* increase (Figure S5A). The TF results reconstruct a general lowering of the palaeomarsh surface through time, while the VA reconstructions suggest lowering of the palaeomarsh surface up-profile from the base of the sequence and relative stability towards the surface. A sample of *Empetrum nigrum* and Cyperaceae seeds from 14-13 cm yielded an age of 210 ± 35 ^{14}C yr B.P. (SUERC-20021, 310-138 cal yr B.P. (78.5 %), 1640-1812 A.D.).

IG1-S1-1

The lithology is dark brown peat overlain by a sand and silt-rich salt marsh peat. The lowermost diatoms are dominated by *Pinnularia intermedia* and *Navicula pusilla* but they decline and are replaced by *N. peregrina* and *Navicula salinarum* up core (Figure S5B). The TF reconstructions are not reliable since they show an increase in palaeomarsh surface elevation up-core, with an abrupt emergence between 12-11 cm. The TF is strongly influenced by the large numbers of *Fragilariforma virescens* in the lower part of the profile, which is found predominantly in the modern environment on the low marsh and tidal flat (Figure S2). Their presence means the TF predicts a low palaeomarsh surface for a deposit that, based on the presence of the indicator species *P. intermedia* and the %LOI data, formed in a high marsh environment. The sudden increase in palaeomarsh surface elevation between 12-11 cm is caused by a fall in frequencies of *F. virescens* at this level. We therefore have greater confidence in the VA reconstructions at the base of the profile, which place more weight on the presence of high marsh species and less on *F. virescens*. The VA reconstructions suggest lowering of the palaeomarsh surface up-profile with relative stability in the top few cm. A sample of *Empetrum nigrum* seeds from 17-16 cm yielded an age of 170 ± 37 ^{14}C yr B.P. (SUERC-27678, 295-124 cal yr B.P. (65.8 %), 1655-1826 A.D.).

IG1-S1-5

The lithology is a dark brown humified peat overlain by slightly silty high salt marsh peat. The diatoms throughout are dominated by *P. intermedia* with smaller quantities of *F. virescens* and *N. peregrina* (Figure S5C). The TF results reconstruct a high palaeomarsh surface at the base of the sequence with lowering up-profile followed by a rise again at the surface. This profile also has relatively large quantities of *F. virescens* throughout which influences TF reconstructions, and we therefore have greater confidence in the VA reconstructions which place more weight on the presence of high marsh diatom species. The VA reconstructs a relatively stable palaeomarsh surface elevation throughout the profile. A sample of *Empetrum nigrum* and Cyperaceae seeds from 5-4 cm yielded a 'modern' ^{14}C age (SUERC-21173).

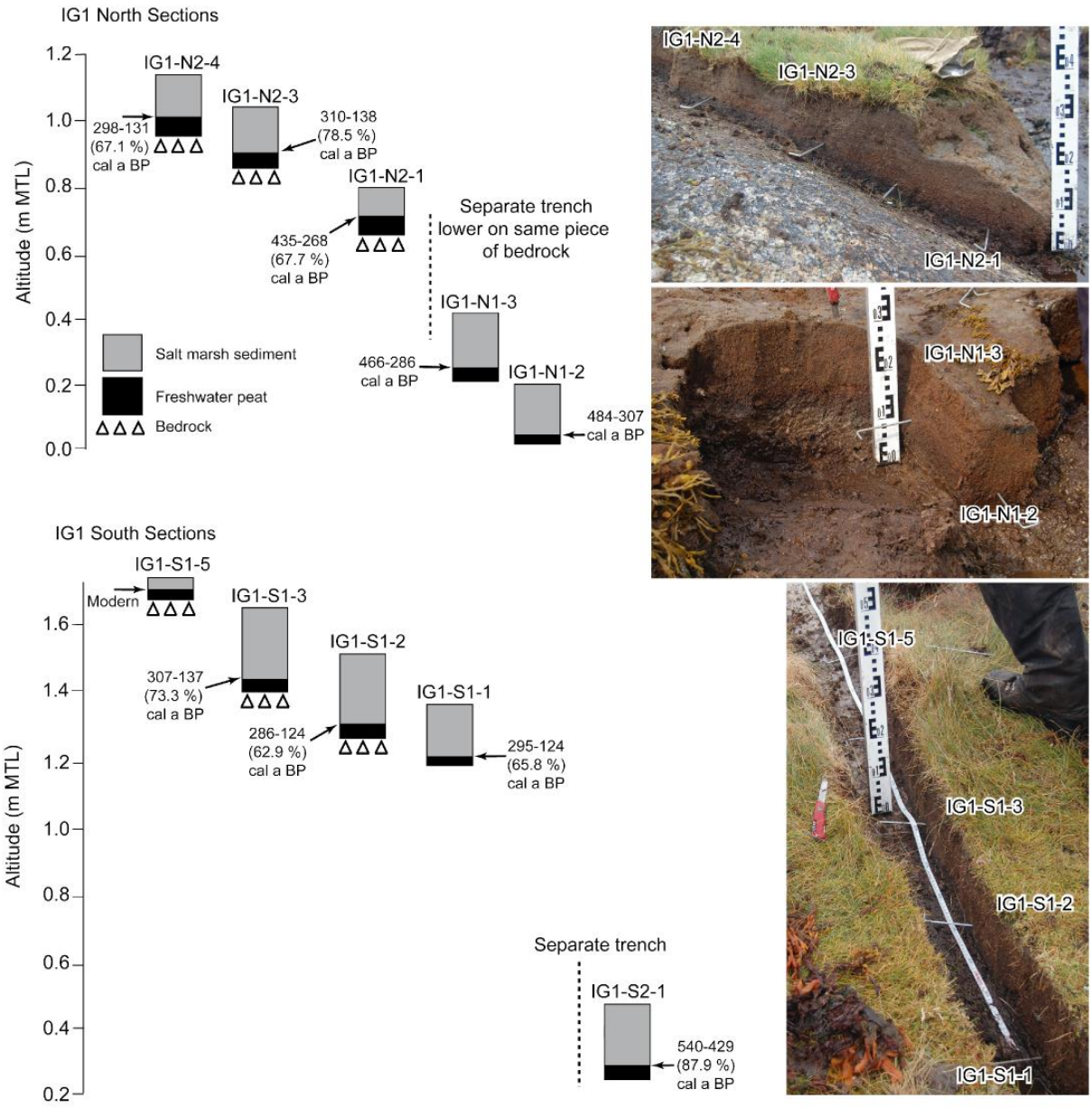

Figure S4. Stratigraphic data from marsh sections at Nanortalik showing the relative location and height range of sample sequences.

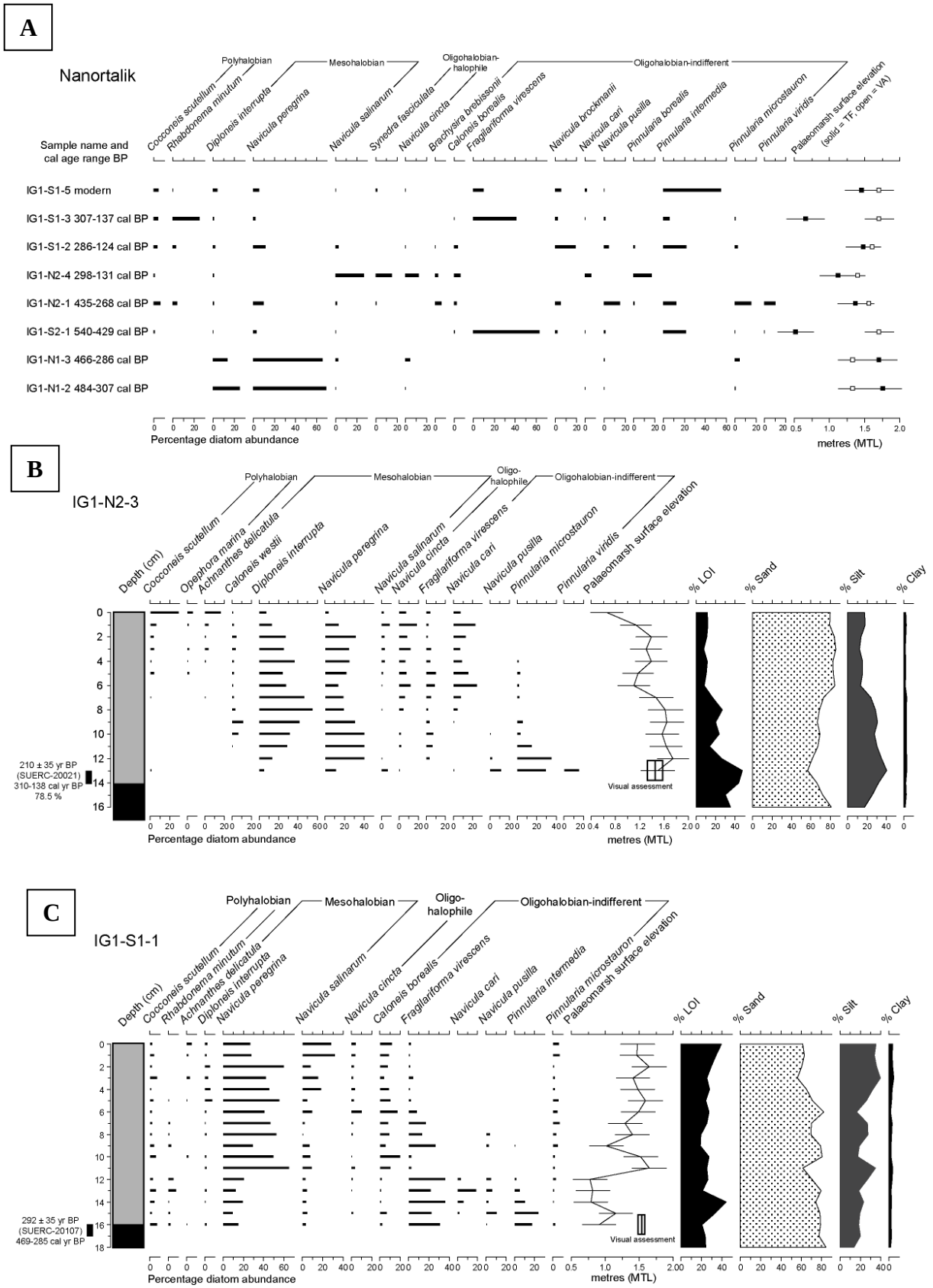

Figure S5 A) Individual diatom samples with radiocarbon dates from Nanortalik marshes. B) diatom profile from section IG1-N2-3 showing transfer function palaeomarsh surface reconstructions and the visual assessment reconstruction for the dated level C) diatom profile from section IG1-S1-1 showing transfer function palaeomarsh surface reconstructions

and the visual assessment reconstruction for the dated level. In each diagram counts are expressed as a percentage of total diatom valves (%TDV) and only data >5% TDV are shown. Radiocarbon dates are listed in full in Table 2 of the main paper.

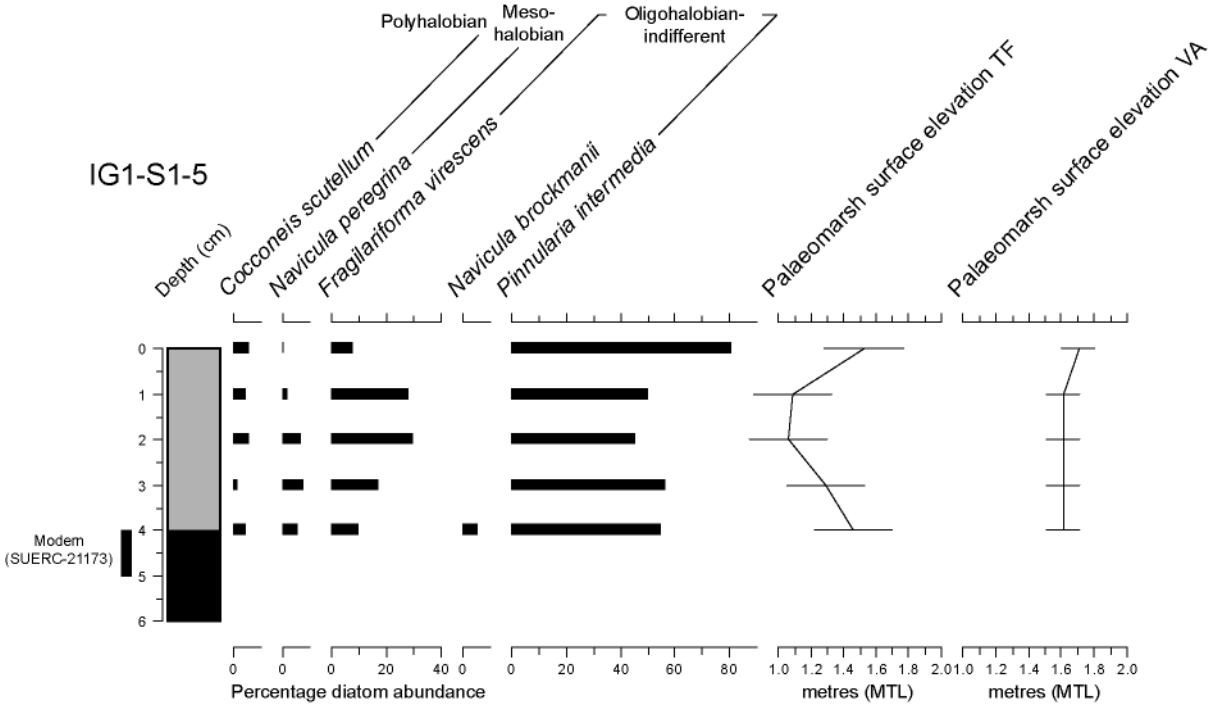

Figure S6. Diatom profile from IG1-S1-5 showing recent RSL stability at Nanortalik. Transfer function results are not reliable from this section because of the high abundance of *Fragilariforma virescens* in the diatom counts. This species is found in low marsh and mudflat environments today (Figure S2) but in fossil samples is often found in association with *Pinnularia intermedia* and other high marsh diatom species. We therefore rely on a Visual Assessment of each sample in this core to reconstruct palaeomarsh surface and RSL change through time.

2. Aasiaat

The field sites at Aasiaat are located on the eastern end of the island of Aasiaat and c. 6 km to the southeast of Aasiaat town on Saqqarliup Nunaa (Figure S7A). We collected modern diatom samples from two marshes (A06/marsh 1 and T08/marsh 3 (details in Woodroffe and Long 2010)) and fossil samples from both Aasiaat island and Saqqarliup Nunaa locations. Dated samples are A06/M1/4, A06/M1/5, A06/M2/1, A06/M2/3, A06/M2/7 from Aasiaat island and T08/M1/1, T08/M1/3, T08/M1/4, T08/M1/7, T08/M2/1, T08/M2/3, T08/M3/1, T08/M3/2 and T08/M4/2 from the Tasiusaq inlet area (Figure S8). Two profiles (AA3 (A06/M2/3) and AA7

(A06/M2/7)) are published in Woodroffe and Long (2010), and we present below a further two (A06/M2/2 and A06/M2/6) (Figure S8).

A06/M2/2

The profile comprises a dark brown well-humified freshwater peat overlain by a more silt-rich salt marsh peat. Diatoms suggest a relatively stable palaeomarsh surface elevation through the profile, dominated by *P. intermedia* with lesser percentages of *Navicula brockmanii* and *Nitzschia palea* (Figure S8B). The TF confirms this suggestion, with slightly decreasing palaeomarsh surface elevation between 5-3 cm. The VA interpretation broadly agrees with this reconstruction at the dated level (7-8 cm depth). A sample of *Empetrum nigrum* and Cyperaceae seeds from 8-7 cm yielded an age of 259 ± 35 ^{14}C yr B.P. (SUERC 17059, 454-271 cal yr B.P. (77 %), 1496-1679 A.D.).

A06/M2/6

The profile comprises a dark brown well-humified freshwater peat overlain by sand-rich salt marsh peat. Diatoms show the up-profile replacement of the high marsh species *P. intermedia* by *D. interrupta, N. peregrina* and *N. salinarum* taxa, representing a low marsh environment (Figure S8C). The TF predicts a relatively stable palaeomarsh surface elevation with a slightly higher level at the dated level (6-7 cm). The VA method places more weight on the presence of the indicator taxon *P. intermedia* and predicts a palaeomarsh surface elevation for the dated level equivalent to the top of the modern *P. phyryganodes* salt marsh environment. A sample of *Empetrum nigrum* and Cyperaceae seeds from 7-6 cm yielded an age of 490 ± 35 ^{14}C yr B.P. (SUERC 16537, 555-496 cal yr B.P. (93 %), 1395-1454 A.D.).

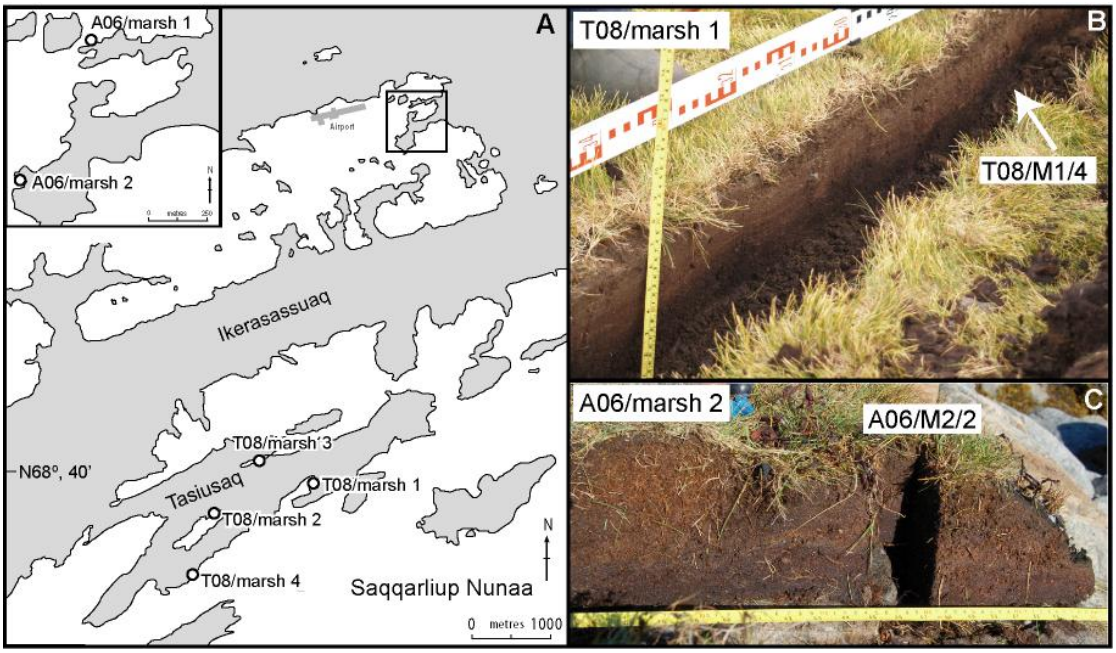

Figure S7 A) location map of the Aasiaat area B) stratigraphy of a trench dug at T08/marsh 1 indicating the generalised stratigraphy seen at all locations (dark brown freshwater peat overlain by mid brown salt marsh peat) and the location of sample section T08/M1/4 C) stratigraphy of a section over bedrock at A06/marsh 2 indicating the location of sample section A06/M2/2.

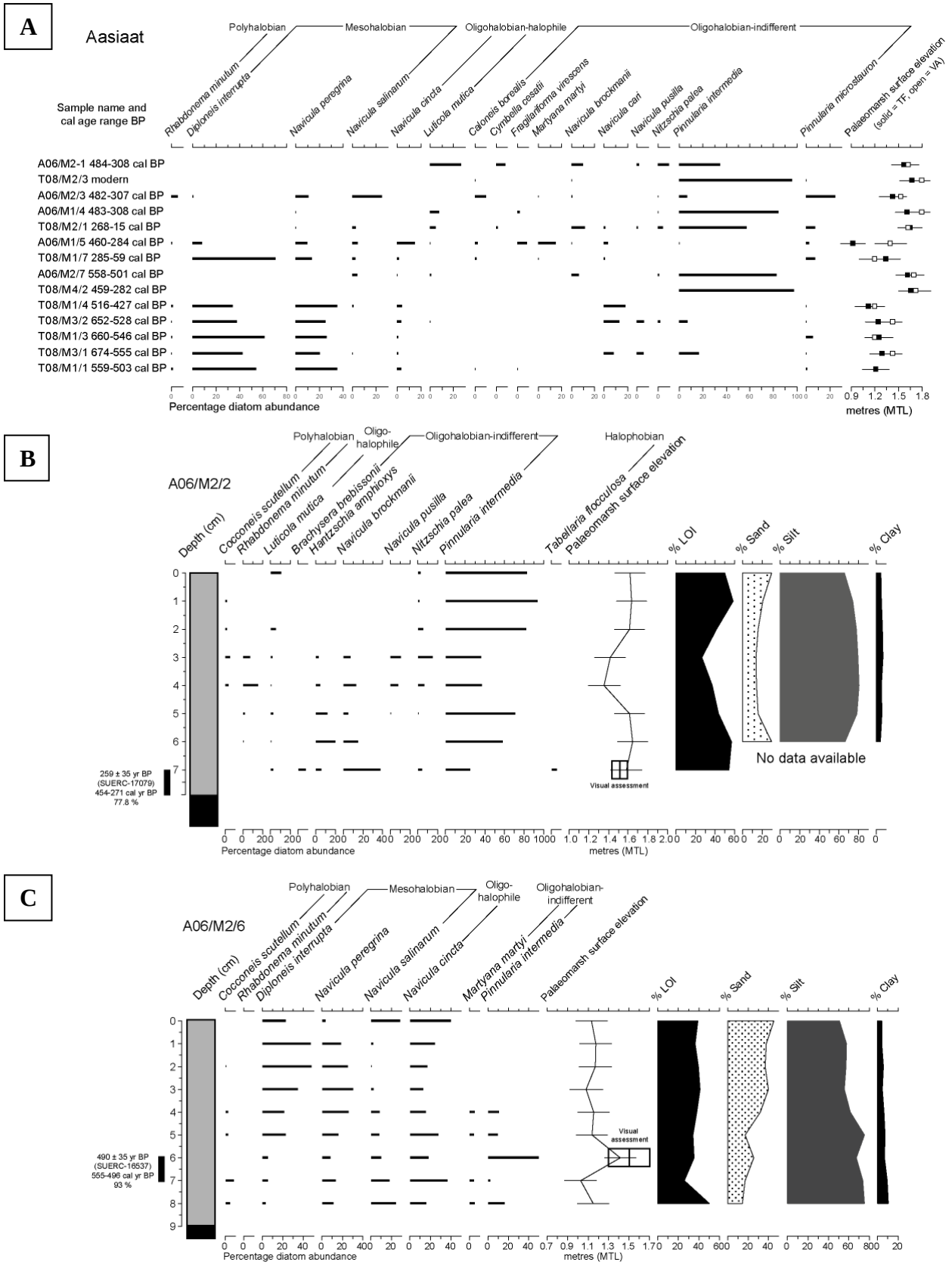

Figure S8 A) Individual diatom samples with radiocarbon dates from Aasiaat marshes. B) diatom profile from section A06/M2/2 showing transfer function palaeomarsh surface reconstructions and the visual assessment reconstruction for the dated level C) diatom profile from section A06/M2/6 showing transfer function palaeomarsh surface

reconstructions and the visual assessment reconstruction for the dated level. In each diagram counts are expressed as a percentage of total diatom valves (%TDV) and only data >5% TDV are shown. Radiocarbon dates are listed in full in Table 2 of the main paper.

Sample number	Sample elevation (m MTL)	Visual Assessment reconstruction criteria (range refers to presence of diatom species above 5 % TDV)	Palaeomarsh surface elevation (m MTL) Visual Assessment	RSL reconstruction (m MTL) Visual Assessment	Palaeomarsh surface elevation (m MTL) Transfer Function	RSL reconstruction (m MTL) Transfer Function	Age range (cal. yr AD) Interpolated = single values
IG1/S1/5	1.71 (surface)	*Navicula peregrina* present (1.51 to 0.91 m MTL range) *Navicula brockmanii* present (1.71 to 1.01 m MTL range) *Pinnularia intermedia* present (1.91 to 1.51 m MTL range)	1.71 (surface)	0 (present MTL)	1.53 ± 0.24	0.18 ± 0.25	2007
	1.70		1.61 ± 0.10	0.09 ± 0.10	1.09 ± 0.24	0.61 ± 0.25	n/a
	1.69		1.61 ± 0.10	0.08 ± 0.10	1.06 ± 0.24	0.63 ± 0.25	n/a
	1.68		1.61 ± 0.10	0.07 ± 0.10	1.29 ± 0.24	0.39 ± 0.25	n/a
	1.67(dated)		1.61 ± 0.10	0.06 ± 0.10	1.46 ± 0.24	0.21 ± 0.25	Modern
IG1/S1/3	1.43 (dated)	*Pinnularia intermedia* present (1.91 to 1.51 m MTL range)	1.71 ± 0.20	-0.28 ± 0.21	0.65 ± 0.27	0.78 ± 0.28	1643-1813
IG1/S1/2	1.32 (dated)	*Navicula peregrina* present (1.51 to 0.91 m MTL range) *Navicula brockmanii* present (1.71 to 1.01 m MTL range) *Pinnularia intermedia* present (1.91 to 1.51 m MTL range)	1.61 ± 0.10	-0.29 ± 0.11	1.49 ± 0.24	-0.17 ± 0.25	1664-1826
IG1/S1/1	1.38 (surface)	*Navicula peregrina* present (1.56 to 0.91 m MTL range) *Pinnularia microstauron* present (1.61 to 1.33 m MTL range) *Caloneis borealis* present (1.71 to 1.38 m MTL range) No *Pinnularia intermedia* (1.91 to 1.51 m MTL range)	1.38 (surface)	0 (present MTL)	1.48 ± 0.27	-0.10 ± 0.28	2007
	1.37		1.36 ± 0.05	0.01 ± 0.06	1.47 ± 0.25	-0.10 ± 0.26	1990
	1.36		1.36 ± 0.05	0 ± 0.06	1.65 ± 0.25	-0.29 ± 0.26	1973
	1.35		1.36 ± 0.05	-0.01 ± 0.06	1.41 ± 0.25	-0.06 ± 0.26	1957
	1.34		1.36 ± 0.05	-0.02 ± 0.06	1.48 ± 0.25	-0.14 ± 0.26	1940
	1.33		1.36 ± 0.05	-0.03 ± 0.06	1.60 ± 0.25	-0.27 ± 0.26	1924
	1.32		1.36 ± 0.05	-0.04 ± 0.06	1.49 ± 0.25	-0.17 ± 0.26	1907
	1.31		1.36 ± 0.05	-0.05 ±0.06	1.30 ± 0.25	0.01 ± 0.26	1891
	1.30		1.36 ± 0.05	-0.06 ± 0.06	1.40 ± 0.25	-0.10 ± 0.26	1874
	1.29		1.36 ± 0.05	-0.07 ± 0.06	1.02 ± 0.25	0.27 ± 0.26	1857
	1.28		1.36 ± 0.05	-0.08 ± 0.06	1.53 ± 0.25	-0.25 ± 0.26	1841
	1.27	*Navicula peregrina* present (1.56 to 0.91 m MTL range) *Pinnularia microstauron* present (1.61 to 1.33 m MTL range) No *Pinnularia intermedia* (1.91 to 1.51 m MTL range)	1.41 ± 0.09	-0.14 ± 0.10	1.65 ± 0.25	-0.38 ± 0.26	1824
	1.26	*Navicula peregrina* present (1.51 to 0.91 m MTL range) *Pinnularia intermedia* present (1.91 to 1.51 m MTL range	1.50 ± 0.06	-0.24 ± 0.07	0.78 ± 0.25	0.48 ± 0.26	1808
	1.25	*Navicula peregrina* present (1.51 to 0.91 m MTL range) *Pinnularia intermedia* present (1.91 to 1.51 m MTL range	1.50 ± 0.06	-0.25± 0.07	0.82 ± 0.25	0.43 ± 0.26	1791
	1.24	*Navicula peregrina* present (1.51 to 0.91 m MTL range) *Pinnularia intermedia* present (1.91 to 1.51 m MTL range	1.50 ± 0.06	-0.26 ± 0.07	0.79 ± 0.25	0.45 ± 0.26	1775
	1.23	*Navicula peregrina* present (1.51 to 0.91 m MTL range) *Pinnularia intermedia* present (1.91 to 1.51 m MTL range	1.53 ± 0.06	-0.30 ± 0.07	1.16 ± 0.25	0.07 ± 0.26	1758
	1.22 (dated)	*Navicula peregrina* present (1.51 to 0.91 m MTL range) *Pinnularia intermedia* present (1.91 to 1.51 m MTL range)	1.54 ± 0.03	-0.32 ± 0.04	0.91 ± 0.25	0.31 ± 0.25	1655-1826 (mid 1742)
IG1/N2/4	1.01 (dated)	*Diploneis interrupta* present (1.34 to 0.91 m MTL range) *Navicula peregrina* present (1.56 to 0.91 m MTL range) *Pinnularia microstauron* present (1.61 to 1.33 m MTL range) No *Pinnularia intermedia* (1.91 to 1.51 m MTL range)	1.40 ± 0.11	-0.40 ± 0.12	1.49 ± 0.25	-0.48 ± 0.26	1652-1819

IG1/N2/3	1.03 (surface)		1.03 (surface)	0 (present)	0.66 ± 0.27	0.37 ± 0.28	2007
	1.02	Decrease in palaeomarsh surface from mid point of *Navicula peregrina* (1.13 m MTL) to present surface (1.03 m MTL)	1.05 ± 0.22	-0.03 ± 0.23	1.14 ± 0.25	-0.12 ± 0.26	1985
	1.01		1.07 ± 0.22	-0.06 ± 0.23	1.39 ± 0.26	-0.38 ± 0.26	1963
	1.00		1.09 ± 0.22	-0.09 ± 0.23	1.30 ± 0.26	-0.30 ± 0.27	1942
	0.99		1.13 ± 0.22	-0.14 ± 0.23	1.39 ± 0.26	-0.40 ± 0.27	1920
	0.98	Mid point of *Navicula peregrina* range (1.56 to 0.91 m MTL range)	1.13 ± 0.22	-0.15 ± 0.23	1.17 ± 0.26	-0.19 ± 0.27	1899
	0.97		1.13 ± 0.22	-0.16 ± 0.23	1.10 ± 0.26	-0.13 ± 0.27	1877
	0.96		1.13 ± 0.22	-0.17 ± 0.23	1.47 ± 0.28	-0.51 ± 0.29	1856
	0.95	*Diploneis interrupta* present (1.34 to 0.91 m MTL range) *Navicula peregrina* present (1.56 to 0.91 m MTL range)	1.25 ± 0.20	-0.30 ± 0.21	1.62 ± 0.29	-0.67 ± 0.30	1834
	0.94	*Diploneis interrupta* present (1.34 to 0.91 m MTL range) *Navicula peregrina* present (1.56 to 0.91 m MTL range) Little *Pinnularia intermedia* (1.91 to 1.51 m MTL range)	1.33 ± 0.20	-0.39 ± 0.21	1.65 ± 0.28	-0.71 ± 0.29	1813
	0.93	*Diploneis interrupta* present (1.34 to 0.91 m MTL range) *Navicula peregrina* present (1.56 to 0.91 m MTL range) Little *Pinnularia intermedia* (1.91 to 1.51 m MTL range)	1.33 ± 0.20	-0.40 ± 0.21	1.57 ± 0.27	-0.64 ± 0.28	1791
	0.92	*Navicula peregrina* present (1.56 to 0.91 m MTL range) *Pinnularia microstauron* present (1.61 to 1.33 m MTL range) No *Pinnularia intermedia* (1.91 to 1.51 m MTL range)	1.41 ±	-0.49 ± 0.12	1.63 ± 0.27	-0.71 ± 0.28	1770
	0.91	*Navicula peregrina* present (1.56 to 0.91 m MTL range) *Pinnularia microstauron* present (1.61 to 1.33 m MTL range) No *Pinnularia intermedia* (1.91 to 1.51 m MTL range)	1.41 ±	-0.50 ± 0.12	1.75 ± 0.26	-0.84 ± 0.27	1748
	0.90 (dated)	*Diploneis interrupta* present (1.34 to 0.91 m MTL range) *Navicula peregrina* present (1.56 to 0.91 m MTL range) *Pinnularia microstauron* present (1.61 to 1.33 m MTL range) *Pinnularia intermedia* present (1.91 to 1.51 m MTL range)	1.44 ± 0.11	-0.54 ± 0.12	1.50 ± 0.27	-0.60 ± 0.28	1640-1812 (mid 1727)
IG1/N2/1	0.73 (dated)	*Navicula pusilla* present (1.71 to 1.43 m MTL range) *Pinnularia intermedia* present (1.91 to 1.51 m MTL range) *Navicula peregrina* present (1.56 to 0.91 m MTL range) *Pinnularia microstauron* present (1.61 to 1.33 m MTL range)	1.56 ± 0.05	-0.83 ± 0.07	1.39 ± 0.25	-0.66 ± 0.26	1515-1682
IG1/S2/1	0.27 (dated)	*Pinnularia intermedia* present (1.91 to 1.51 m MTL range)	1.71 ± 0.20	-1.44 ± 0.21	0.52 ± 0.25	-0.25 ± 0.25	1410-1521
IG1/N1/3	0.25 (dated)	*Diploneis interrupta* present (1.34 to 0.91 m MTL range) *Navicula peregrina* present (1.56 to 0.91 m MTL range)	1.33 ± 0.20	-1.08 ± 0.21	1.72 ± 0.25	-1.47 ± 0.26	1484-1664
IG1/N1/2	0.05 (dated)	*Diploneis interrupta* present (1.34 to 0.91 m MTL range) *Navicula peregrina* present (1.56 to 0.91 m MTL range)	1.33 ± 0.20	-1.28 ± 0.21	1.77 ± 0.26	-1.72 ± 0.25	1466-1643
Aasiaat							
A06/M2/1	1.64	*Pinnularia intermedia* present (1.87 to 1.47 m MTL range) *Navicula brockmanii* present (1.78 to 1.28 m MTL range)	1.63 ± 0.15	0.01 ± 0.16	1.56 ± 0.16	0.08 ± 0.17	1466-1642
T08/M2/3	1.64	Only *Pinnularia intermedia* present (1.87 to 1.47 m MTL range, becomes dominant above 1.80 m MTL)	1.80 ± 0.10	-0.16 ± 0.11	1.67 ± 0.15	-0.03 ± 0.16	Modern
A06/M2/2	1.52	*Pinnularia intermedia* present (1.87 to 1.47 m MTL range) *Navicula brockmanii* present (1.78 to 1.28 m MTL range) (Lower than AA1 as more species diversity)	1.52 ± 0.16	0.00 ± 0.17	1.58 ± 0.16	-0.06 ± 0.17	1496-1679
A06/M2/3	1.43	*Pinnularia intermedia* present (1.87 to 1.47 m MTL range) *Pinnularia microstauron* present (1.82 to 1.48 m MTL range) *Navicula peregrina* present (1.43 to 0.63 m MTL range) *Navicula salinarum* present (1.58 to 0.53 m MTL range)	1.43 ± 0.05	0.00 ± 0.07	1.48 ± 0.18	-0.05 ± 0.19	1468-1643

A06/M1/4	1.39	Dominated by *Pinnularia intermedia* (1.87 to 1.47 m MTL range, becomes dominant above 1.80 m MTL)	1.80 ± 0.10	-0.41 ± 0.11	1.61 ± 0.16	-0.22 ± 0.17	1467-1642
T08/M2/1	1.38	*Pinnularia intermedia* present (1.87 to 1.47 m MTL range) *Navicula brockmanii* present (1.78 to 1.28 m MTL range)	1.63 ± 0.15	-0.25 ± 0.07	1.64 ± 0.15	-0.26 ± 0.16	1665-1891 1682-1935
A06/M1/5	1.23	*Navicula peregrina* present (1.43 to 0.63 m MTL range) *Diploneis interrupta* present (1.43 to 0.57 m MTL range) *Navicula cincta* present (1.37 to 0.63 m MTL range) No *Pinnularia intermedia* (1.87 to 1.47 m MTL range) *Pinnularia microstauron* present (1.82 to 1.48 m MTL range)	1.40 ± 0.20	-0.17 ± 0.21	0.93 ± 0.16	0.30 ± 0.17	1490-1666
A06/M2/6	1.13	*Pinnularia intermedia* present (1.87 to 1.47 m MTL range) *Navicula peregrina* present (1.43 to 0.63 m MTL range) *Diploneis interrupta* present (1.43 to 0.57 m MTL range) *Navicula cincta* present (1.37 to 0.63 m MTL range)	1.50 ± 0.20	-0.37 ± 0.21	1.42 ± 0.15	-0.29 ± 0.16	1395-1454
T08/M1/7	1.04	*Diploneis interrupta* present (1.43 to 0.57 m MTL range) *Navicula peregrina* present (1.43 to 0.63 m MTL range)	1.20 ± 0.20	-0.16 ± 0.21	1.34 ± 0.17	-0.30 ± 0.18	1665-1891
A06/M2/7	1.03	*Navicula peregrina* present (1.43 to 0.63 m MTL range) Few other minor species present	1.70 ± 0.12	-0.67 ± 0.13	1.62 ± 0.15	-0.59 ± 0.16	1392-1449
T08/M4/2	0.93	Dominated by *Pinnularia intermedia* (1.87 to 1.47 m MTL range, becomes dominant above 1.80 m MTL)	1.80 ± 0.10	-0.87 ± 0.20	1.66 ± 0.15	-0.73 ± 0.16	1491-1668
T08/M1/4	0.63	*Diploneis interrupta* present (1.43 to 0.57 m MTL range) *Navicula peregrina* present (1.43 to 0.63 m MTL range)	1.20 ± 0.20	-0.57 ± 0.14	1.14 ± 0.17	-0.51 ± 0.18	1434-1523
T08/M3/2	0.54	*Diploneis interrupta* present (1.43 to 0.57 m MTL range) *Navicula peregrina* present (1.43 to 0.63 m MTL range) *Pinnularia intermedia* present (1.87 to 1.47 m MTL range)	1.42 ± 0.13	-0.88 ± 0.14	1.26 ± 0.16	-0.72 ± 0.17	1298-1422
T08/M1/3	0.52	*Diploneis interrupta* present (1.43 to 0.57 m MTL range) *Navicula peregrina* present (1.43 to 0.63 m MTL range)	1.20 ± 0.20	-0.68 ± 0.14	1.26 ± 0.16	-0.74 ± 0.17	1290-1404
T08/M3/1	0.49	*Diploneis interrupta* present (1.43 to 0.57 m MTL range) *Navicula peregrina* present (1.43 to 0.63 m MTL range) *Pinnularia intermedia* present (1.87 to 1.47 m MTL range)	1.42 ± 0.13	-0.93 ± 0.14	1.31 ± 0.16	-0.82 ± 0.17	1276-1395
T08/M1/1	0.33	*Diploneis interrupta* present (1.43 to 0.57 m MTL range) *Navicula peregrina* present (1.43 to 0.63 m MTL range)	1.20 ± 0.20	-0.87 ± 0.14	1.23 ± 0.16	-0.90 ± 0.17	1391-1447